A Simple and Efficient Pipeline for Construction, Merging, Expansion, and Simulation of Large-Scale, Single-Cell Mechanistic Models

Cemal Erdem[1,*], Ethan M. Bensman[2], Arnab Mutsuddy[1], Michael M. Saint-Antoine[3], Mehdi Bouhaddou[4], Robert C. Blake[5], Will Dodd[1], Sean M. Gross[6], Laura M. Heiser[6], F. Alex Feltus[7,8,9], and Marc R. Birtwistle[1,10,*]

[1] Department of Chemical & Biomolecular Engineering, Clemson University, Clemson, SC

[2] Computer Science, School of Computing, Clemson University, Clemson, SC

[3] Center for Bioinformatics and Computational Biology, University of Delaware, Newark, DE

[4] Department of Cellular and Molecular Pharmacology, University of California San Francisco, San Francisco, CA

[5] Center for Applied Scientific Computing, Lawrence Livermore National Laboratory, Livermore, CA

[6] Department of Biomedical Engineering, Oregon Health & Sciences University, Portland, OR

[7] Department of Genetics and Biochemistry, Clemson University, Clemson, SC

[8] Biomedical Data Science and Informatics Program, Clemson University, Clemson, SC

[9] Center for Human Genetics, Clemson University, Clemson, SC

[10] Lead Contact

[*] Correspondence: cemalerdem@gmail.com (C.E.) and mbirtwi@clemson.edu (M.R.B.)

ABSTRACT

The current era of big biomedical data accumulation and availability brings data integration opportunities for leveraging its totality to make new discoveries and/or clinically predictive models. Black-box statistical and machine learning methods are powerful for such integration, but often cannot provide mechanistic reasoning, particularly on the single-cell level. While single-cell mechanistic models clearly enable such reasoning, they are predominantly “small-scale”, and struggle with the scalability and reusability required for meaningful data integration. Here, we present an open-source pipeline for scalable, single-cell mechanistic modeling from simple, annotated input files that can serve as a foundation for mechanistic data integration. As a test case, we convert one of the largest existing single-cell mechanistic models to this format, demonstrating robustness and reproducibility of the approach. We show that the model cell line context can be changed with simple replacement of input file parameter values. We next use this new model to test alternative mechanistic hypotheses for the experimental observations that interferon-gamma (IFNG) inhibits epidermal growth factor (EGF)-induced cell proliferation. Model-based analysis suggested, and experiments support that these observations are better explained by IFNG-induced SOCS1 expression sequestering activated EGF receptors, thereby downregulating AKT activity, as opposed to direct IFNG-induced upregulation of p21 expression. Overall, this new pipeline enables large-scale, single-cell, and mechanistically-transparent modeling as a data integration modality complementary to machine learning.

INTRODUCTION

The ever-increasing availability and accumulation of FAIR (1) (findable, accessible, interoperable, and reproducible) big (omics) datasets requires new computational methods and models to integrate, analyze, and interpret the underlying information. A central question in biomedical science moving forward is related to "data integration" (2–4): How can we leverage the totality of available information not only to learn more about biology but also to make predictions, especially those that are clinically relevant? Advances in statistical and machine learning approaches enable (mostly) data-driven exploration and hypothesis generation from big datasets (5–8). Trained on features of the input dataset(s), such models can be used for, as just a few examples, to predict drug responses (9–11) or decide tumor type/stage (12–15). Although transformative, such machine learning and statistical models have shortcomings. Most notably, they often fail to explain predicted outcomes with detailed mechanistic reasoning (16–20) – a major scientific gap and a roadblock to reconciling and integrating such models. Moreover, they often do not explicitly consider single-cells—a fundamental building block for scaling models up and down as needed, as well as an accelerating thrust of current big data generation efforts.

Besides such "black-box" modeling approaches, an alternative and complementary vehicle for data integration are so-called "mechanistic models" (20). A fundamental feature of mechanistic models is that they are based on a set of biophysical assumptions about the system and cellular processes (21), which usually gives rise to systems of differential equations. Mechanistic models provide an interpretable integration of different data types, because they have explicitly modeled biophysical correlates, while enabling further exploration for underlying logic behind heterogeneous, nonlinear, and often unintuitive relationships across big datasets. If mechanistic models are available towards the whole-genome or whole-single-cell scale, one can start to predict complex, multi-network, and emergent cellular behaviors (22,23), elucidate phenotypic responses to multiple perturbations (24,25), tailor and train on patient-specific data for personalized, pharmacologic decision making (26,27), or just use them as "data integrators" for data consistency checking (28).

However, most published mechanistic models are "small" scale; built for single pathways with a handful of genes, meant to interpret a single dataset (29–38). Such small-scale mechanistic models provided important insights into processes such as yeast response to pheromones (35), *lac* operon regulation in *E. coli* (34), or phenotypic responses to different ligand stimulations (29). For instance, Vilar et al. (34) showed that a computational model can explain phenotypic inheritance (*lac* induced or uninduced) of *E. coli* cells when stochasticity and population level

responses are incorporated into the model. However, the limited scope of the small-scale models means they inherently will struggle to integrate multiple datasets. Large-scale mechanistic models (23,39–41), on the other hand, can provide a more extensive representation of cellular interactions and are thus well-poised for data integration.

Currently, mechanistic models are constructed in two main ways. The first uses existing models and modifies them with additional mechanisms by inserting new species or interactions to explain new experimental observations (38,42,43). Using the same network and changing the cellular context can also be considered within this scope (40). Model merging, the act of stitching pre-existing models together, is an extension of this method for creating larger models. However, such an approach requires extensive detail checking and harmonizing species/parameter definitions. Often, unfortunately, sufficient annotation is not provided which makes this task harder. Moreover, while most mechanistic models are comprised of ordinary differential equations (ODEs), many large-scale models require multiple sub-modules of different mathematical formalisms. For example, metabolic processes are usually described by steady-state flux-balance models (44,45), gene expression events are stochastic (46–48), and protein signaling events are represented by a system of ODEs (29,30,38). Thus, sorting out a single platform for different modeling formalisms to create a large-scale model is a daunting task. It is so far only achieved by creating highly custom-structured and custom-coded model-agglomerates that are not well-suited to further alterations or re-use (23,40).

The second way of constructing models is to build them bottom-up by writing out every reaction one by one. In this regard, rule-based modeling (RBM) provides an innovative approach (49). All RBM software, such as BioNetGen (50,51), Kappa (52), and PySB (53), enable researchers to write “rules” for *repeated* reaction events following certain patterns. RBM software then creates the reaction network by propagating the rules from the initial set of species. Although RBM revolutionized large-scale model construction by minimizing manual equation scripting (i.e. writing out every differential equation), there are some limitations. First, it can generate a very large (even infinite) number of reactions from a small set of rules (usually called *the curse of combinatorial complexity*). This makes interpreting, analyzing, and debugging such models cumbersome, if possible. Tools like NFsim (54) can overcome such problems by simulating events based on the rules, rather than *a priori* generating the entire reaction network. Such software thus becomes advantageous when a small number of rules create a very large number of reactions, e.g. polymerization, aggregation, or multi-site phosphorylation (55). However, such network-free simulators typically require an explicit representation of every molecule in the

system, which greatly increases the computational cost and renders such methods inefficient for large-scale mechanistic models. Secondly, RBM dictates that reactions taking place via the same rule have the same rate constant parameter values. Often, allostery or site cooperativity precludes this simplifying assumption, which then leads to manually writing out every such reaction in the model (or writing one rule for each reaction), which then obviates the advantages of RBM.

Regardless of how a large-scale model is constructed, it should have certain properties for FAIRness (findable, accessible, interoperable, and reproducible) and re-useability (56–58). Porubsky et al. (57) recently summarized the *best modeling practices* and reinforced: providing metadata/annotations and model creation steps/files (Practices 1-5), using standard and cross-platform model files (Practice 3), and open-source, license-free, version-controlled, and reproducible model dissemination (Practices 8-9). As the size of the model increases, conforming to modeling standards (e.g. simulation type, simulation speed, software to use, scripting package to use, algorithm to use) gets harder. That is why most of the large-scale (many genes or whole-cell) models are necessarily custom-structured, are composed of multiple submodules, or are lacking sufficient annotations and metadata (e.g. ENSEMBL or HGNC identifiers) (23,39–41). These custom-made models also do not yet follow a single standard format, a key property for easy distribution, re-use, and model merging and expansion with other models. The SBML (Systems Biology Markup Language) format (59,60) offers a long-established and well-defined way of specifying annotated model structures, with an explicit and structured definition of each element of a mechanistic model (species, reactions, volumes, initial concentrations, parameters, rules, events, equations). SBML is an extensible, machine-readable markup language and not a simple text file. SBML has interfaces and packages in most programming languages (like Python, C++, Perl) and can be imported by most software (Python, MATLAB, COPASI (61), Virtual Cell (62), and another ~300 packages). However, it is non-trivial to write thousands of reactions in SBML standards, directly or with available GUI-based software. To circumvent this problem, there are efforts to convert other model formats to SBML, like Antimony (63). The Antimony format is defined in simple text format and is human readable and interpretable.

Any constructed mechanistic model, in SBML format or not, must be simulated with reasonable CPU time. Although simulating models on local machines is often done, High Performance (HPC) or Cloud Computing (CC) platforms are suitable for larger tasks such as parameter sensitivity/estimation or multiple single-cell simulations (64–67). Therefore, another milestone for large-scale mechanistic models is to become HPC/CC compatible, especially for single-cell simulations and heterogeneous data integration.

Here, we develop a new framework for large-scale mechanistic modeling that helps move towards addressing the substantial gaps noted above. First, we define a simple set of structured and annotated input text files that set model specifics: genes, species, reactions, reaction stoichiometry, cellular compartments, transcriptional regulations, input omics data, and parameter values (Fig. 1). These text files enable easy creation or alteration of the model network, without any coding or software usage requirements (but they are easily amenable to such things if desired). We then use Jupyter notebooks (68) to process the input files and to create a human-interpretable Antimony file, which is then converted into an SBML (community gold-standard) model file. We simulate the model using SBML compatible Python packages including AMICI, specifically designed for faster and parallel (HPC/CC compatible) simulation settings (67,69), and our own Python submodule for stochastic gene expression that enables single-cell simulations with large mechanistic models.

We also develop an HPC/CC (Kubernetes) compatible version of the pipeline that is specifically designed for simulation settings with large number of single cells or stimulation conditions. The proposed framework thus simplifies large-scale mechanistic model merging and variant creation, providing opportunities for easy data consistency checking and candidate mechanism selection. As a test case, we convert and extend one of the largest single mammalian cell mechanistic models of proliferation and death signaling and regulation (40,70–76), which we call SPARCED (**S**BML, **P**roliferation, **A**poptosis, **R**eceptor Tyrosine Kinases, **C**ell cycle, **E**xpression, **D**NA damage). The pipeline and model are available on GitHub (github.com/birtwistlelab/SPARCED). Using the newly created model format, we explore different mechanisms to explain the experimental observation that interferon-gamma (IFNG) inhibits epidermal growth factor (EGF)-induced cell proliferation. Our model analysis suggests, and experiments support the hypothesis that IFNG inhibits cell proliferation through SOCS1-induction and reduced AKT activity, rather than by IFNG-induced p21 expression upregulation. This large-scale mechanistic model construction framework and the model outlined here is an important step towards creating and testing large-scale mechanistic models as data integration and clinical decision-making tools.

METHODS

Computational Methods

The Bouhaddou2018 model

The Bouhaddou2018 model (Fig. 1A) is one of the largest single-cell mechanistic models for mammalian cell signaling regulating proliferation and death. The first version of the model used as a test case in this work was written in MATLAB (The MathWorks, Inc.) (40). The model is a hybrid of deterministic and stochastic modules. The deterministic module describes the concentration dynamics of 774 proteins, protein complexes, and post-translationally modified species through 2449 reactions using the Sundials CVODEs package for simulation (77). The stochastic module describes gene state (active/inactive) and mRNA birth/death dynamics for 141 genes. The deterministic and stochastic modules exchange information every 30 simulated seconds. In short, the current levels of select protein states can induce changes in gene activation/deactivation and/or mRNA transcription/decay rates. The newly updated mRNA copy numbers change nascent protein translation rates in the deterministic module. See (40) for further details.

The SPARCED model

We converted the Bouhaddou2018 model into a Python + SBML (59) format (Fig. 1B). The deterministic module is ultimately encoded in an SBML file (.xml) whereas the stochastic module is written in Python. A foundational and important feature of this recoding effort is that the SBML file is generated from a small set of simple structured input text files (Fig. 1C) via Python scripts. Introduction of such structured input files and associated Jupyter notebooks enables simple alteration of model structure and/or parameter values, for example turning on/off certain interactions. The input files also enable rigorous annotation of model features using, for example, ENSEMBL (78) and HGNC (79) identifiers, which is seldom done in such mechanistic modeling.

Input files

There are six SPARCED model input text files (tab separated values), each with a defined structure as detailed below. The user can change these files to create and compile a new model.

(1) `OmicsData`: This file (Table S1) includes the gene copy number and mRNA copy number data. Total protein abundance data can also be included in this file if available, but all protein level information is currently embedded in the initial species concentration values in the Species input file. Making use of total protein abundance data and converting these values into protein and protein complex starting concentrations is possible, as introduced by *Initialization* protocol in

Bouhaddou2018 model. This SPARCED version does not yet perform initialization but rather uses the default MCF10A context values as a starting point for model alterations. This input file also contains rate constants for the stochastic module. Each row of the file corresponds to one gene and the columns are different data types. The first column is gene name (HGNC identifiers), the second column is gene copy number, the third column is mRNA molecule copy number per cell (mpc), the fourth and fifth columns are rate constants of gene inactivation and activation respectively (s^{-1}), the sixth column is constitutive transcription rate constants (molecules per second), the seventh column is maximal transcription rate constants (molecules per second), and finally the eighth column is mRNA degradation rate constants (s^{-1}). The rate constants are taken from the Bouhaddou2018 model. Users can add new rows to this file, using RNAseq data to estimate mRNA levels for the genes to be added (40). When adding genes (rows) to the model, a reasonable starting point for rate constants (or other values), in the absence of any other data, is to use median values from the genes/parameters currently in the model.

(2) `Species`: This file (Table S2) contains information about the species in the deterministic module. Each row corresponds to one species (protein, protein complex, post-transcriptionally modified species). Transcripts (in nM) are also included in this file because they are regarded as species with updated concentrations in the stochastic module every 30 seconds and are used in translation rate laws. The first column is the species name. Names can be arbitrary so long as they are unique in the model. Importantly, the name list needs to match the first column in the `StoichiometricMatrix` file described below. The second column is the species home compartment. The home compartment of a species defines its cellular localization. A species can reside in a compartment defined in the `Compartments` input file: currently Cytoplasm, Mitochondria, Nucleus, or Extracellular. The third column is initial condition in nM units, with respect to the home compartment volume. These values are taken from the Bouhaddou2018 model, post-initialization. The fourth column is a comma separated list of ENSEMBL gene identifiers corresponding to gene products present in the species.

(3) `Ratelaws`: This file (Table S3) has a row for each reaction in the deterministic module. The first column is the unique (arbitrary) name of each reaction. Currently, we named each reaction based on the related sub-module (e.g. vA1-87 for Apoptosis and vC1-104 for Cell Cycle). The number and order of rows in this file should match the columns in the `StoichiometricMatrix` input file defined below. The second column in this file contains the home compartments for the reactions. The designated compartments should be one defined in the `Compartments` input file: currently Cytoplasm, Mitochondria, Nucleus, or Extracellular. The home reaction compartments

define the effective search volume for each reaction and is used to rescale concentrations when appropriate. Note that both species and reactions have home compartments defined, where a species can participate in a reaction defined in a different compartment. For instance, the EGF binding to EGFR reaction occurs in extracellular space (volume V_e), where EGF's home compartment is the extracellular space and EGFR's home compartment is cytoplasm (V_c). A volumetric correction for EGFR concentration in this rate law is done by multiplying by the ratio of V_c/V_e. The third column can have either a number or a reaction formula. If it is a number, it means the corresponding reaction is mass-action type, and the number is the rate constant for that reaction in units of nM and seconds. Note that the reactants and products are defined in the `StoichiometricMatrix` input file. If the third column is a formula, it means the reaction will follow that rate law, and the next set columns in that row are the values of each parameter defined in the formula in the third column, again in units of nM and seconds. The rate law can include any species name described in the Species input file. The parameter names in the rate law should start with "*k*" and be unique in that formula. We distinguish multiple parameter names with an underscore and ascending list of numbers (e.g. kA_1, kA_2). During model generation, all parameter names in this file are re-named in an ascending order based on the number of rate laws. The full list of parameter name/value pairs are outputted into a new file (`ParamsOut`) for user reference.

(4) `StoichiometricMatrix`: This file (Table S4) defines the reaction stoichiometry, and therefore the reactants and products of model reactions. The rows correspond to the `Species` input file and the columns correspond to the rows in the `Ratelaws` input file. Here, the species and rate law names should match the names defined in Tables S2 and S3. Each element (starting at the second row and second column index) has a stoichiometric coefficient (typically -2, -1, 0, 1, or 2), where negative sign indicates reactants, and positive sign implicates products of a reaction.

(5) `GeneReg`: This file (Table S5) describes transcriptional activation and inhibition interactions, where rows correspond to genes (the same order as the first column of Table S1) and columns to species that are defined as activators or repressors of transcriptional activity. The first column is gene name (HGNC format). There are currently seven more columns in this file, each corresponding to one species defined as an activator or a repressor (e.g. p53 induces p21 transcription or AP1 inhibits cFOS transcription). A single value of zero indicates no effect. A non-zero entry in row i and column j denotes that species j regulates gene i transcription. The non-zero entries have the form "A; B", where "A" is the hill coefficient and "B" is the half-maximal

concentration of the species “j” effect. To simplify the input file structure, we use positive values of “A” to denote activation, and negative “A” values to denote inhibition. This file is used by the stochastic module script to update mRNA levels. To add additional transcriptional regulators (activators or repressors) into the SPARCED model, users should add as many columns as new regulator species and populate the columns with corresponding rate constants.

(6) `Compartments`: This file (Table S6) contains the names of compartments in the model (first column), the volume of the compartment in liters (second column), and the corresponding GO-term of the compartment (third column). The compartment names should match the compartment names listed in `Species` and `Ratelaws` input files.

Dependencies

(1) `Docker`: All model dependencies and runtime environments are *Dockerized* into a downloadable image for self-contained model execution. To run the SPARCED model using Jupyter notebooks (SPARCED-jupyter), Docker must be installed. Then, by downloading the docker image, built on the Ubuntu-18.04 operating system with `python3` installed (hub.docker.com/repository/docker/ebensma/sparced), users can run the Jupyter notebooks defined below in any web-browser within the docker container. The Docker image includes system utilities required for the simulation package `AMICI` (67,69).

Jupyter notebook 1: model creation

The input files described above are processed by the “`createModel`” Jupyter notebook (68) (Supp. File 1) and converted into an Antimony (63) text file (Fig. 1B and Supp. File 2). This intermediate step and file provide an additional means to model input, fine-tuning, and alteration for experienced users. It can be explored via any text editor and it lists all elements of the model: species, rate laws, parameters, compartments, and corresponding values (Supp. File 2). This text file is then converted into an SBML (.xml) file, using `libantimony` in the same script. The Antimony format does not, to our knowledge, support addition of structured annotations, so the annotations (species and compartments) are added to the newly created SBML file using `libsbml` and the model input files (Tables S2 and S6). Finally, the annotated SPARCED model file (.xml) is generated (Supp. File 3).

Deterministic module

The model SBML file forms the basis of the deterministic module. When run deterministically, the model does not account for stochastic gene switching and mRNA transcription events (see next

section). The default parameters and concentrations of the SPARCED model correspond to an average, serum-starved cell state in deterministic mode.

Stochastic module

In addition to the deterministic module, the SPARCED model includes a stochastic module. The stochastic module describes gene states (active/inactive) and mRNA birth/death events for genes (currently 141 of them). The deterministic and stochastic modules exchange information every 30 simulated seconds. The current levels of select protein states can induce changes in gene activation/deactivation and/or mRNA transcription/decay rates. The newly updated mRNA copy numbers change nascent protein translation rates in the deterministic module. See (40) for further details.

The stochastic module constitutes two short Python scripts. At the start of each simulation, one of the scripts (`RunPrep.py`) reads in the `OmicsData` input file, processes parameter values, and sets the initial transcript levels and stochastic module rate constants. The second script (`SGEmodule.py`) uses information from `RunPrep.py` and species concentrations from the deterministic module to simulate mRNA transcription/degradation and gene activation/inactivation events. One output of the second script is the new concentrations of mRNAs, which is updated in the deterministic module to calculate rates of translation for the next 30 second simulation. The second output is the state of all gene copies (active or inactive).

Jupyter notebook 2: model simulation

Supp. File 4 includes an example of simulation setup and input parameters of the SPARCED model. The notebook "`runModel`" imports a user specified model SBML file and stochastic module scripts to run simulations using the `AMICI` package (69,80). `AMICI` is an interface for `Sundials CVODEs` solvers that converts SBML files into executable C code for fast simulation. Other required input parameters for model simulation include: a flag to specify if the simulations are fully deterministic (flag=1) or hybrid (flag=0), the total simulation time in hours (th), input ligand concentrations, and a flag (1 or 0) to indicate if results should be exported.

The SPARCED-I model

SPARCED-I model creation

We created a new enlarged version of the SPARCED model called SPARCED-I. We merged Yamada2003 model (81) of interferon-gamma receptor (IFNGR) signaling into SPARCED. The expansion included addition of 34 new species, 8 corresponding genes, and ~70 reactions. New genes (IFNG, IFNGR, JAK2, STAT1, SHP2, SOCS1, PPN, PPX) corresponding to the proteins in

the model are added as new rows and mRNA levels are inserted into the `OmicsData` input file. Gene copy numbers are taken as two (40). Each new protein, protein complex, and mRNA species are inserted into the `Species` and `StoichiometricMatrix` input files as new rows. Each new reaction is inserted into the `Ratelaws` input files as rows, and into the `StoichiometricMatrix` input file as new columns. The new genes are added as rows to the `GeneReg` file. The final SPARCED-I model has 954 species and 2540 reactions.

Parameter estimation of the SPARCED-I model

After expansion of the SPARCED model with IFNGR pathway and setting the initial species levels from MCF10A cells, SPARCED-I model showed ultrafast receptor and STAT1 activation dynamics inconsistent with biological observations. Thus, we selected six rate constant parameters for calibration based on substantial sensitivity for STAT1 activation dynamics. The parameters calibrated are: (i) STAT1 binding to activated receptor complexes, (ii) nuclear translocation rate of STAT1* dimers, (iii) SOSC1 mRNA translation rate constant, (iv) SOCS1 protein degradation rate, (v) STAT1 unbinding rate from active receptor-SOCS1 complexes, and (vi) set the EIF4E-dependent translation rate constant of SOCS1 to zero (see (40) for details on the EIF4E effect on translation). We fit the chosen parameters individually, while keeping the values of "best fit" at each step. The range of variation was set at ±2 in log10 scale. The SPARCED-I model was then run 1000 simulated hours, without any ligand stimulation, for equilibration.

Context estimation of the SPARCED-I model

The SPARCED model initial conditions are based on serum and growth factor starved MCF10A cells, grown in standard tissue culture plates. However, the experiments involving IFNG were done in media with horse serum and collagen-coated tissue culture plates. The details of both experimental procedures are explained below. "Bridge" experiments showed that the horse serum upregulates active AKT (ppAKT) levels four-fold prior to growth factor stimulation. We modeled increased basal levels of active AKT with IGF1 treatment for 24 hours, and found that 0.02 nM IGF1 was consistent with the above experimental observations (Fig. S15). Therefore, we simulate the SPARCED-I model with 0.02 nM IGF1 treatment for 24 hours prior to EGF or EGF+IFNG stimulation.

Cell proliferation estimation in SPARCED-I model

The Bouhaddou2018 model used cyclin A levels as a proxy for cell cycle entry in each cell (40). Here, we used the same MATLAB scripts (`findpeaks.m`) as the Bouhaddou2018 model to

identify the peaks in cyclin A trajectories. A peak is defined as a hill-like shape, with a minimum prominence of 4 nM compared to surrounding basal levels. For each cell, the number of occurrences of such peaks are counted within 0-48 hours of simulation. Then, the peak counts in all 100 starting cells are summed to find the total number cell cycles in the population.

SPARCED-nf (nextflow, model version running on Nautilus-Kubernetes cluster)

The SPARCED model can be ported to high-performance cloud computing infrastructures for large-scale simulation, in the SPARCED-nf variant. Specifically, we ran SPARCED-nf simulations using the Pacific Research Platform, a distributed network of academic computing resources organized as a Kubernetes cluster (64,66). The prevalence of Kubernetes on both democratized and commercial cloud compute networks makes the model portable, allowing users to run large-scale jobs on distributed supercomputers on a wide range of platforms (65).

Dependencies

(1) `Docker`: As is the practice with Kubernetes-compatible workflows, all model dependencies and runtime environments are *Dockerized* into a downloadable image for self-contained model execution. This means when a job for SPARCED-nf is launched on the Kubernetes cluster, it will download the Docker image for SPARCED-nf and execute the model within that container. The Docker image for SPARCED-nf is built on the Ubuntu-18.04 operating system with python3 installed, as well as a few minor system utilities required for `AMICI`. The image can be found at https://hub.docker.com/repository/docker/ebensma/sparced.

(2) `Nextflow` (nf): In this cloud-scalable version of the model, the Jupyter notebooks have been converted into python source code and re-modularized for greater parallel-simulation efficiency. The process of creating and executing the model is handled entirely by `Nextflow`, a workflow-management application and language for building resilient pipelines. When SPARCED-nf is launched, `Nextflow` begins by creating a head pod on the cluster to coordinate each of the jobs needed to run the model (Fig. S1). The head pod creates smaller jobs that each download the containerized dependencies from Dockerhub, pull the model source files from the SPARCED-nf GitHub repository, and run the assigned process. Once the model has completed execution, the output files are saved to a section of the Kubernetes cluster called the persistent volume claim (PVC), where they remain stored in the cloud for user download.

SPARCED-nf model simulation set-up

SPARCED-nf uses the same tab-separated-value input files as SPARCED. For SPARCED-nf to build and execute, the files are copied into the aforementioned PVC for workflow access. This is

done with `kube-runner` (https://github.com/SystemsGenetics/kube-runner), a submodule for automating common PVC tasks with Kubernetes' `kubectl` tool. The `kube-load.sh` file is used to write new input to the PVC, and `kube-login.sh` is used to access and delete old input files from the cluster.

Along with its scalability, SPARCED-nf is also highly customizable. The `nextflow.config` configuration file is used to define the specifics of simulation scenarios.

(1) `nextflow.config`: This configuration file has two main sections. In the first section (called K8), users define the Kubernetes namespace specifics and folder configurations. In the second section (called params), users customize runtime arguments for simulation settings. The available parameters are input_dir_name (the directory name of the input files), flag_deterministic (flag=1 for deterministic or flag=0 for hybrid simulations), sim_time (simulation time in hours), Vol_nuclear (volume of nuclear compartment in liters), Vol_cyto (volume of cytoplasmic compartment in liters), speciesVals (species names + initial concentration values to start from), ratelawVals (parameter names + values), and numCells (number of single cells if the simulations are hybrid). Importantly, the "speciesVals" and "ratelawVals" parameters allow users to pass in a formatted string to specify parameter sweeps. Using these in conjunction with the "numCells" parameter, the user can simulate thousands of cells in hundreds of different microenvironments in a single execution.

(2) `SPARCED-nf:model_build`: Analogous to "`createModel.ipynb`" in SPARCED-jupyter model, this phase of the Nextflow pipeline constructs all necessary files for the model simulation.

(3) `SPARCED-nf:split_from_params`: This is the major parallelizing step of SPARCED-nf. Having received the relevant model files from the last step, the workflow ingests the *speciesVals*, *ratelawVals*, and *numCells* arguments set by the user in the `nextflow.config`. Using the input files, it creates new input files to satisfy the user-specified parameter sweeps. Each new input file permutation is moved into its own new folder, and each such folder is duplicated *numCells* times.

(4) `SPARCED-nf:model_run`: This final step of the Nextflow workflow is responsible for model execution and output generation. Each folder created in the previous step above serves as the unique runtime environment in this step. The model pulls assigned simulation input files associated with the folder. Each instance of this step is run in parallel across different simulation environments (Fig. S1B). Functionally, the code executed is very similar to the "`runModel.ipynb`" notebook and the model outputs are saved to the PVC.

When the models complete execution, each `SPARCED-nf:model_run` instance saves its output to a unique folder on the PVC. To download these folders to the local filesystem, users can employ `kube-save.sh` (from the `kube-runner` module).

GitHub

The final model scripts, files, and information are available in Birtwistle Lab GitHub repository (github.com/birtwistlelab/SPARCED).

Experimental Methods

Cell culture and western blotting

Cell culture: MCF10A cells (acquired from LINCS Consortium/Gordon Mills and STR verified internally) are cultured in DMEM/F12 (Gibco #11330032) medium supplemented with 5% (by volume) horse serum (Gibco #16050122), 20ng/mL EGF (PeproTech #AF-100-15), 0.5 mg/mL hydrocortisone (Sigma #H-0888), 10µg/mL insulin (Sigma #I-1882), 100ng/mL cholera toxin (Sigma #C-8052), and 2mM L-Glutamine (Corning #25-005-CI). Cells were cultured at 37ºC in 5% CO2 in a humidified incubator and passaged every 2-3 days with 0.25% trypsin (Corning #25-053-CI) to maintain subconfluency. Serum starvation medium is DMEM/F12 medium supplemented with 2mM L-Glutamine. Experimental starvation medium is DMEM/F12 medium supplemented with 5% (by volume) horse serum (Gibco #16050122), 0.5 mg/mL hydrocortisone (Sigma #H-0888), 100ng/mL cholera toxin (Sigma #C-8052), and 2mM L-Glutamine (Corning #25-005-CI).

Tissue culture treated, non-collagen coated plates with full serum starvation: The cells were seeded in full growth media at 150,000 cells/well in tissue culture treated six well plates (Corning # 08-772-1B). The next day, cells are washed once with 1X PBS (one phosphate buffered saline tablet (Sigma #P4417-100TAB) in 200 mL milli-Q water, autoclaved) and the media was exchanged to serum starvation media (DMEM/F12 medium, 2mM L-Glutamine) for 16-24 hours. Then, the cells were treated with vehicle control, EGF (10 ng/mL, PeproTech #AF-100-15), and HGF (40 ng/mL, R&D Systems #294-HGN-005) for 0, 5, and 60 minutes in a humidified, 5% CO2, 37ºC incubator.

Collagen-coated plates and growth-factor starvation only: Collagen-coating mixture was prepared as follows: 7.5 mL diluent buffer (20% v/v glycerol, 10 mM EDTA, PBS), 1.5 mL Tris-HCL, 0.6 mL COL1 (Cultrex #3442-050-01), and 5.4 mL PBS. 950 µL coating mix was added into each well of a six-well plate. After making sure that the entire well surface was covered, the plates were incubated one hour at room temperature. After incubation, any remaining liquid is aspirated and

discarded. The wells were washed twice with sterile PBS and left lid-open under a sterile laminar flow hood until wells were fully dry (~one hour). Upon replacement of the plate lid, the plates were stored in a benchtop desiccator at room temperature for a minimum of 3 days before use. Then, MCF10A cells were seeded in full growth media at 150,000 cells/well. After being allowed to attach for 7-8 hours, the wells were washed once with PBS and the media was changed to full growth media without EGF and insulin for 18 hours. Then, the cells were treated with vehicle control, EGF (10 ng/mL), and HGF (40 ng/mL) as above for 0, 5, and 60 minutes.

Cell lysis: After growth factor treatment, the plates were removed from the incubator and put on ice. The media in the wells were aspirated and the wells were washed with PBS. 110 µL of freshly-prepared, ice-cold RIPA buffer (50mM Tris, pH 7-8 (Acros Organics #14050-0010) , 150 mM NaCl (Fluka #71383), 0.1 % SDS (Fisher #46040CI), 0.5% sodium deoxycholate, 1% Triton-X-100, filter sterilized, stored at 4C) with protease & phosphatase inhibitors (1µg/mL aprotinin, 1µg/mL leupeptin, 1µg/mL pepstatin A, 10 mM β-glycerophosphate, and 1mM sodium orthovanadate) was added into each well, while gently rotating the plate to cover the full surface area. The plates were transferred to the cold room for 15-20 minutes, with slow rocking. The lysate was scraped off from the wells with a cell scraper. 100 µL of cell lysate from each well were transferred into labeled Eppendorf tubes on ice. Each tube was vortexed three times to homogenize cell debris, keeping other tubes on ice. All tubes were then centrifuged at 4°C for 15 minutes at 14000 rpm. 80 µL of the supernatant from each tube was transferred into new Eppendorf tubes on ice. These cleared lysate samples were stored at -80C for long-term storage or used immediately as below.

Protein quantification: Total protein quantification was done using the BCA-Pierce 660 Assay (Thermo Scientific #23225). As the reference, BSA stock (Thermo Scientific #23209) was used according to the manufacturer protocol. In short, 10 µL of samples and BSA standards were loaded into wells, in triplicate, in a 96-well plate (Corning #3370). 150 µL BCA Protein Assay Reagent was loaded into each non-empty well. The plate was covered and incubated at room temperature for 5 minutes. The absorbance at 660 nm was measured on a plate reader (BioTek #Epoch2). The average reading of blank wells was subtracted from all other readings, and then average readings were calculated. The standard curve was fitted by a polynomial using blank-corrected mean values of each standard condition versus its BSA concentration. The fitted curve was used to determine the protein concentration in each sample.

Immunoblotting and quantification: The lysates were put on ice and the amount of sample to load into each well was calculated using the total protein concentrations determined above (3 µq loaded here). Each sample was mixed with 2X Sample Buffer (950 µL of Laemmli's Buffer (BioRad

#161-0737), 50 µL beta-mercaptoethanol (Fisher #03446I-100)) in a 1:1 ratio and transferred into a new Eppendorf tube. The sample solutions was heated at 95°C for 5min on the heating plate and then briefly spun in benchtop microcentrifuge to return any condensation to the bottom of the tube. 10% acrylamide gels were prepared, and samples were loaded into the wells. A pre-stained protein ladder (LI-COR #928-70000) was loaded in the first and last wells. The gel was run in SDS running buffer (100 mL 10X Tris-Glycine-SDS buffer (IBI Scientific #IB01160) + 900 mL milli-Q water) at constant 220V until the dye front runs off the gel. Then, wet-transfer to nitrocellulose membrane (0.45µm pore size, VWR #10063-173) was done using cold transfer buffer (3.03g Tris-base (Acros Organics #14050-0010), 14.4g glycine (Acros Organics #220910050), 100 mL methanol (BDH #BDH1135-4LP), volume adjusted to 1 Liter with milli-Q water) and running the cassette with ice block at constant 100V for one hour. 1X TBST (Tris-Buffered Saline, 0.1% Tween) was prepared: 100 mL of 10X TBS solution (24 g Tris-base, 88 g NaCl (Fluka #71383), adjusted pH to 7.6, adjusted final volume to 1 Liter with milli-Q water, autoclaved), 1 mL Tween-20 (Fisher #BP337-100), and milli-Q water until final volume of 1 Liter (~900 mL). When the transfer was finished, the membrane was blocked using BSA-TBST blocking buffer (2.5 g bovine serum albumin (Fisher# BP1600-100), 50 mL 1X TBST) for 45min at room temperature. The blocking buffer was discarded, and the membrane is incubated in primary antibody solution (1:1000 dilution, 10 µL primary antibody in 10 mL 5% BSA-TBST blocking buffer) overnight in cold room. The primary antibodies used were: AKT_pS473 (Cell Signaling #4060; 1:1000), AKT (Cell Signaling #2920; 1:1000), ERK_pT202_pY204 (Cat: 4370; 1:1000), ERK (Cell Signaling #4696; 1:1000), alpha-tubulin (Novus #NB100-690, 1:1000), and β-actin (LI-COR #926-42212, 1:1000). After primary antibody incubation, membranes were washed three times for 15 min each with 1X TBST at room temperature, with gentle rocking. Then, the membranes are incubated with LI-COR secondary antibodies in 10 ml TBST blocking buffer for 45 minutes (anti-rabbit 800CW, LI-COR #926-32211 or anti-mouse 680LT, LI-COR #925-68070; 1:8000) at room temperature, with gentle rocking. Membranes was washed three times for 15 min each, with 1X TBST, on rocker. The imaging was done with a LI-COR Odyssey Infrared Imager, where bands were quantified using LI-COR Image Studio Lite v5.2 software (Figs. S14-17).

RESULTS

SPARCED Model Construction and Unit Testing

Current large-scale mechanistic models are agglomerates of smaller models and tools, used mainly within the same research lab. Most such models also lack clear and satisfactory annotation and metadata, making them harder to understand and alter (23,40). The goals of this work were (i) to build a foundation for large-scale mechanistic model construction and alteration, that is simple, efficient, open-source, and cloud computing compatible and (ii) to provide a scalable and re-useable big mechanistic model for a single mammalian cell.

Our pipeline starts with creating a set of simple input files for one of the broadest cancer signaling models in the literature (40), called the Bouhaddou2018 model here (Fig. 1A). The input files are simple tab-separated text files (Fig. 1B-C), unlike licensed file formats with a mixture of hard coded information in multiple interconnected scripts commonly used in modeling literature. A Jupyter notebook processes the input files into an Antimony text file (Supp. File 2). The model creation code generates the SPARCED model file in SBML format (Supp. File 3) using the Antimony text file and annotations from the model input files (Tables S2 and S6). When the model construction step is complete and the SBML file is created, it is imported and simulated using a Python package called AMICI (67,69).

We demonstrate the use of this format by constructing a large-scale model named SPARCED. The SPARCED model only requires modifying the structured input files (Fig.1B) to define the entire model, including network topology and the values of model parameters and species concentrations. Like the Bouhaddou2018 model, the initial SPARCED model is based on non-transformed breast-epithelial MCF10A cell line data. We annotated all the species in the model with ENSEMBL gene identifiers, providing easier programmatic filtering and curation of species list, while keeping the user defined simpler names for complicated species structures. After creation of the new SPARCED model files, we verified that the previous Bouhaddou2018 model simulations are reproducible and match expected experimental observations through the same unit test concept (Table 1) introduced for the original model (40). Each unit test has a dedicated Jupyter notebook on GitHub repository (github.com/birtwistlelab/SPARCED/SPARCED_Brep). We illustrate select unit testing examples below, but all results are presented in supplementary figures (Figs. S2-11).

The SPARCED model consists of two modules: deterministic and stochastic. The SBML file forms the basis of the deterministic module whereas the stochastic module describes gene states (active/inactive) and mRNA birth/death events for the genes. When run in the hybrid simulation

mode, the deterministic and stochastic modules exchange information every 30 simulated seconds. The current levels of select protein states can induce changes in gene activation/deactivation or mRNA transcription/decay rates. The newly updated mRNA copy numbers change nascent protein translation rates in the deterministic module. When run deterministically, the model does not stochastically sample gene activation or mRNA transcription events, and such simulations correspond to an average cell state.

SPARCED model Unit Testing: deterministic

We first tested deterministic SPARCED model simulations. The SPARCED model simulations recapitulated the response of an average (deterministic) cell under different stimulation conditions, to within simulation error (Fig. 2A). As an example, we highlight SPARCED model simulations of the cell response (MCF10A cells) to treatment with EGF alone or EGF+insulin (Figs. 2B and S12). Treating growth factor and serum-starved MCF10A cells with EGF and insulin induces activation of AKT and ERK, which together control cell proliferation (40,73,74). The Bouhaddou2018 model showed that compared to single ligand treatments, EGF+insulin stimulation increases and prolongs AKT and EIF4EBP1 phosphorylation (p) (Fig. 2B). The simulation results from the Bouhaddou2018 model (the solid lines) and SPARCED model (circles) are indistinguishable. The SPARCED-nf implementation, which runs on a high-performance cloud computing infrastructure, similarly reproduces the original simulation data (Fig. 2B, also solid lines). These results, together with all other deterministic tests in Table 1 (Figs. S3-8 and 11), confirm that the SPARCED model recapitulates the Bouhaddou2018 model simulations and unit tests in deterministic settings. Thus, the simple input file structure combined with automatic model generation is equivalent to the prior MATLAB instantiation.

SPARCED model Unit Testing: stochastic

Next, we evaluated the SPARCED model for stochastic unit tests in single cell simulations. Each single cell (simulation) has different initial protein levels and dynamics due to stochastic gene expression, and thus may respond differently to the same treatment. The SPARCED model stochastic simulations closely matched Bouhaddou2018 model results, to within simulation error (Figs. 2C and S13A). As an example, we highlight here how single cells respond stochastically to DNA damage. Etoposide, a chemotherapy drug, induces double- and single-stranded DNA damage, causes cell cycle arrest, and leads to cell death (82). Experiments showed that in the absence of EGF and insulin (to promote cell cycle exit), there is minimal etoposide-induced cell death (Fig. S13B-C) (40). However, in the presence of EGF and insulin (to drive cell cycle progression), etoposide-induced cell death increases over time and reaches around 60% of the

cells (Fig. 2D-E). Simulating etoposide treatment of cycling cells induces robust p53 pulses, disruption of Cyclin A dynamics/cell cycle arrest (Fig. 2D), and more cell death relative to non-cycling cells (Fig. 2E). These results closely match experimental data and Bouhaddau2018 simulations. We conclude that SPARCED model captures DNA damage induced single-cell death percentage and cell cycle state-dependent effect of etoposide. The SPARCED model also passed all other stochastic unit tests (Table 1, Figs. S2, 6,7,9, and 10).

SPARCED model Unit Testing: context change

Different cell types have different expression levels, and many mechanistic models assume that it is different expression levels that drive different phenotypes, not changes in biochemical constants. These constants are based on biophysical events like binding, which are based on molecular structures. Here, we tested the ability of the SPARCED model to be re-"initialized" to study different cell types by changing initial levels of total proteins and mRNAs without changing the model topology. Thus, we introduced a protocol to enable SPARCED model context change (Fig. 3A and Table 2). In short, `OmicsData`, `Species`, and `Ratelaws` input files are updated with new cell line information, including mRNA levels, protein/species levels, and constitutive translation rate constants. Then, the new model is created by running the "`createModel`" Jupyter notebook or by submitting a new SPARCED-nf job.

The re-calibration step for context change followed in Bouhaddou2018 model was called *Initialization*, where protein specific translation rates and key parameters important for cell decision making were recalculated to make sure that the model reaches steady state and that reproduced expected phenotypic behavior with respect to proliferation and apoptosis. To test the drug combination response differences in different cell lines, we changed SPARCED model context (i.e. parameter values and species concentrations) using the *Initialized* set of values for U87 glioma cell line from Bouhaddou2018 model. Following the protocol outlined in Fig. 3A, we replaced MCF10A cell line values in the input files with values from U87 cell line data.

U87 cells are PTEN-deficient and more sensitive to AKT inhibition compared to MCF10A cells (40). Both cell lines show minimal sensitivity to MEK inhibition alone and AKT & MEK inhibitors are both needed to kill MCF10A cells. In contrast, AKT inhibition alone is sufficient to kill U87 cells. To simulate the U87 cell response to AKT and MEK inhibitors, we first updated the `OmicsData` input file (Table S1) using U87 mRNAseq data from Bouhaddou2018 model (Supp. File 5). We set PTEN translation rate to zero and set values of rate parameters dictated by *Initialization* in the `Ratelaws` input file (Fig. 3B and Table S7). We also updated the species initial

conditions in `Species` input file using steady-state values for U87 cells from the Bouhaddou2018 model. We created a new model SBML file (SPARCED_U87) using the updated input files. SPARCED_U87 model simulations of response to MEK and AKT inhibitors reproduced the Bouhaddou2018 model results and experimental observations (Fig. 3C). We conclude that changing model context by changing input files accomplishes the goal of easy model alteration to study of different cell types.

Illustrating easy model expansion an application to the IFNG pathway: SPARCED-I

The SPARCED model reproduces original model results and experimental observations, but how can we use the new simple model expansion capabilities? Here, we focused on experimental observations that interferon-gamma (IFNG) inhibits MCF10A cell proliferation. Specifically, as part of a much larger LINCS consortium effort to deeply profile the MCF10A cell line dynamic response to perturbations (synapse.org/#!Synapse:syn12526172), we observed that IFNG inhibits EGF-induced cell proliferation (Fig. 4A). We wanted to use the SPARCED model expansion functionality to evaluate the suitability of candidate mechanisms by which IFNG might inhibit proliferation.

We thus merged a model for interferon-gamma receptor (IFNGR) signaling into SPARCED, creating the model variant SPARCED-I. The newly added Yamada2003 model (81) captures how IFNG binds to pre-JAK-bound receptors, inducing dimerization. The ligand-bound receptor homodimers are activated by JAK, which also phosphorylates STAT1 when bound to the active receptor complex. Activated STAT1 then dimerizes and translocates to the nucleus, inducing transcription of SOCS1. SOCS1 mRNA is exported to the cytoplasm and are translated into SOCS1 protein. SOCS1 protein binds to and inhibits activated receptor homodimers. In this model, there are three phosphatases (SHP2, PPX, and PPN) acting on multiple species.

Following the model alteration protocol in Fig. 3A and Table 2, we added 34 new species, 8 corresponding genes, and ~70 reactions (Fig. 4B) based on the Yamada2003 model (81). New genes (IFNG, IFNGR, JAK2, STAT1, SHP2, SOCS1, PPN, PPX) corresponding to the proteins in the model are added as new rows and mRNA levels are inserted into the `OmicsData` input file. Gene copy numbers are taken as two (40). The genes are also added as new rows to the `GeneReg` file (Table S8). In the Yamada2003 model, activated nuclear STAT1 dimers (STAT1*Dn) induce SOCS1 mRNA transcription and this is captured by adding a new column in the `GeneReg` input file, with the only non-zero element at the STAT1*Dn and SOCS1 gene intersection. Next, each protein, protein complex, and mRNA species are inserted into the

`Species` and `StoichiometricMatrix` input files as new rows. Each new reaction is inserted into the `Ratelaws` input files as rows, and into the `StoichiometricMatrix` input file as new columns. This expansion brought the total number of species of SPARCED-I model to 954, and the number of reactions to 2540 (Fig.4C, Table S9).

SPARCED-I model Unit Testing

The SPARCED-I model, with parameter values from the Yamada2003 model, should reproduce the original results exactly, which we verified (Fig. 4D, red lines & diamonds, respectively). We then modified the mRNA, protein, and compartment volume values to that of MCF10A cell context (data from (40)). However, the MCF10A data (Table S10) had missing values for IFNGR and (arbitrary) phosphatase species PPN and PPX. So, we initialized the concentration of IFNGR as half of JAK2 concentration (the receptor is typically rate limiting (81)). The concentrations of PPN and PPX phosphatases were equal to half of SHP2 concentration in Yamada2003 model, so we updated their values to half of SHP2 concentration in MCF10A cells. In addition to the reactions from the Yamada2003 model, we added new translation (for the new eight genes) and degradation (for all new species) reactions into the model. The rate constants of these extra reactions are initially assumed to be equal to the average of corresponding reactions of SPARCED model genes. Starting from these parameter values, the SPARCED-I model showed unrealistic (ultrafast) receptor activation and STAT1 phosphorylation/nuclear transport rates. Therefore, we varied six parameters that have high impact on STAT1 activation dynamics (see Methods) to approximate the timing (within the first hour) of STAT1*Dn pulses reported in Yamada2003 model (Fig. 4D) and others (83,84). Changing rate constants in such a manner accounts for the entangled effects of unmodeled (i) cellular context and (ii) mechanisms. Tuning these parameters produced expected pulsing times and response behavior of STAT1*Dn, SOCS1, and SOCS1 mRNA levels (Fig. 4D black lines). The final values are updated in the SPARCED-I model file (Supp. File 6).

A key feature of SPARCED-I is its ability to simulate single cell behavior and the above-observed reduction in proliferation induced by IFNG is inherently a single cell property. As a unit test, we simulated 100 single cell trajectories (Fig. 4E) of SPARCED-I model and concluded that SPARCED-I model recapitulates observations from earlier models and passes all unit tests.

SPARCED-I model variant analysis: hypotheses testing

Next, we wanted to use the expanded model to help us interpret the experimental observations. H*ow does IFNG inhibit EGF-induced cell proliferation?* The SPARCED model captures regulation of cell proliferation via the ERK and AKT pathways. Growth inducing ligands, like EGF, bind to

and activate receptor tyrosine kinases (RTKs), which in turn leads to upregulation of AKT and ERK phosphorylation. The two pathways together induce upregulation of cyclin D through cJUN, cFOS, and cMYC activities (40,73,85).

In the literature, there are different mechanisms by which IFNG was suggested to play a role in cell proliferation and death (86–89). The SPARCED-I model enabled us to evaluate these hypotheses for consistency with experimental observations (Fig. 4A), where the simulation steps are matched to the experimental setup (Fig. 5A). The first proposed mechanism (mech 1, Fig. 5B) was based on reports that activated STAT1 can induce p21 (cell cycle inhibitor) expression (86,90). This mechanism was modeled (Supp. File 7) by modifying the `GeneReg` input file (Table S9), where active STAT1 dimers can increase p21 transcription rate. The SPARCED-I model already had p21 transcriptional activation by p53, and the rate constant for transcriptional activation of p21 by STAT1 was taken to be equal to the parameter values from the p53 mechanism.

The second mechanism involves the negative regulator of IFNG signaling, SOCS1. SOCS1 protein has different binding domains, including SH2 domains (91,92). SH2 domains bind to phosphorylated tyrosine residues on other proteins (93,94). It is proposed that SOCS1 not only binds to activated IFNG receptors, but also to many other activated receptor complexes with free phosphorylated tyrosine residues (mech 2, Fig. 5C) (92,95,96). Thus, IFNG-induced SOCS1 protein can bind to growth factor-activated receptor complexes (or the so-called signaling competent dimers – pSCD) and prevent further downstream signaling by sequestration. This mechanism was modeled by adding SOCS1 binding to activated receptor complexes (pSCDs) reactions in the `Ratelaws` input file. The SPARCED-I mech2 model contained 1302 species (348 new) and 3584 reactions (1044 new) (Supp. File 8). GRB2 proteins also contain SH2 domains that bind to tyrosine phosphorylated receptors (pSCDs) and the rate constants of SOCS1 interaction with all these complexes are taken as the average of such parameters of GRB2 complexes.

Before evaluating these model variants, the initial conditions must be set. The SPARCED-I model initial conditions are based on serum and growth factor starved MCF10A cells. However, the experiments with IFNG (Fig. 4A) were done in media with horse serum. Horse serum upregulates ppAKT levels by four-fold (Figs. S14 and S15), possibly thorough IGF/IGF1R pathway (97–99). Including 0.02 nM IGF meets this basal activity increase constraint, and therefore is included in simulations prior to and during simulated EGF and IFNG treatments (see Methods and Figs. S14-17).

After creating the SPARCED-I Mechanism 1 and 2 variants and defining the simulation conditions, we stochastically simulated both models with IGF treatment for 24 hours for 100 different single cells. Then, either EGF or EGF + IFNG are added for an additional 48 hours for each cell (Fig. 5A). As a simulation metric for cell proliferation, we counted and summed the number of cyclin A peaks in each of the 100 starting cells for the duration of 48 hours (Fig. 5D and E-orange and blue bars). Mechanism 2 leads to a significant decrease in the number of cell cycles in IFNG treated cells, whereas Mechanism 1 did not cause a change in EGF and EGF+IFNG conditions.

Exploring further, we saw that Mechanism 1 did not lead to significant increases in p21 protein levels (area plots in Fig. 5F). While it is unexpected that the model predicted no significant increase in p21 levels despite a clearly added mechanism, if the parameter value for STAT1 induction of p21 transcription is changed enough (see Supplemental E12 in (40)), simulations do indeed show IFNG treatment induces p21 (Fig. S18). However, experimental RPPA data from the LINCS Consortium confirm that total p21 levels do not significantly change over the course of 48 hours in EGF+IFNG treated cells compared to EGF alone stimulation (error bars in Fig. 5F, synapse.org/#!Synapse:syn12526172). We conclude that the original parameter choices are appropriate and that the putative p21 mechanism is therefore unlikely.

We investigated responses of simulated cells with Mechanism 2 to explore why fewer simulated cells enter the cell cycle (Fig. 5E). We saw that AKT phosphorylation was lower in IFNG treated cells, compared to only EGF stimulated cells (Fig. 5G area plots). The greatest decrease occurs at around one hour after stimulation and stays decreased for 48 hours. We compared this simulation result to experimental RPPA data (synapse.org/#!Synapse:syn12526172), which also show decreased ppAKT levels at 1-4 hours post-ligand treatment (Fig. 5G error bars). The rest of the time points (8, 24, and 48 hours) did not show a significant difference between EGF alone and EGF + IFNG cases. We also saw a decrease in MAPK activation in IFNG treated cells, in both Mechanism 1 and 2, which is supported by experimental data (Fig S19). But is the somewhat subtle decrease in AKT activity enough to prevent cell cycle entry in MCF10A cells? Bouhaddou et al. showed that a slight change in time integrated AKT dynamics can tilt the cell cycle progression decisions significantly (see Fig. S11 and (40) for further details) and here we saw ppAKT levels show a statistically significant decrease after IFNG treatment, which may explain fewer proliferative cells. Taken together, these results suggest that: (1) the SPARCED model formalism can be used for simple implementation of large-scale mechanistic model-based hypotheses testing, (2) STAT1 induction of p21 expression levels is an unlikely mechanism in this

MCF10A cell context, (3) crosstalk between IFNG and EGF pathways may occur through SOCS1 sequestration of activated receptor domains, and (4) SOCS1-induced inhibition of AKT activation may contribute to proliferation suppression.

DISCUSSION

Here, we have introduced a mechanistic model construction pipeline that enables large-scale, single-cell modeling as a data integration tool using simply structured, annotated input files and open-source software. Our pipeline is based on structured and easy to modify input text files and uses Jupyter notebooks or scripts (for scaled cloud-computing) to create and simulate model files. It also enables easy model alteration (species/rate law or parameter value changes), omics data integration, and model variant vs. hypotheses testing. Our first application of this pipeline, the SPARCED model, is available online on GitHub (github.com/birtwistlelab/SPARCED). SPARCED can serve as a basis for both creating context-specific (personalized) model variants and as a building block towards whole-cell-scale models.

First, we showcased the use of SPARCED model by changing the cellular context of the model from MCF10A breast epithelial cells to U87 glioblastoma cells, by only replacing parameter values in three input files. Although we used previously calculated values from the Bouhaddou2018 model, it is notable that SPARCED pipeline correctly creates and simulates a large-scale mechanistic model file only from an altered set of input files. Secondly, we investigated two candidate mechanisms to explain how IFNG can inhibit EGF-induced cell proliferation. By creating and testing two mechanisms (by only changing the input files), we hypothesized that IFNG-induced SOCS1 sequestration of activated receptors is a more likely mechanism than IFNG induction of cell cycle inhibitor protein p21. Besides these two mechanisms tested, there are others in the literature, like the positive feedback of STAT1 inducing STAT1 and IRF1 transcription (87), or the inhibition of Bcl-2 by STAT1 (86). However, here, we only focused on demonstrating the capabilities of SPARCED pipeline to easily create and test model variants to help explain one of our experimental observations, where testing all possible mechanisms was out of our scope.

Many existing big models are constructed in complicated and hard-coded ways and are not available in standard modeling formats, like SBML. For instance, the Bouhaddou2018 model we used as our starting point was custom coded in MATLAB with tens of different script files with thousands of lines. Although the model performance was optimized for its topology, alteration and expansion of the model was practically impractical. However, models, especially the large-scale and clinically relevant mechanistic models, must become easy to formulate, understand, and disseminate for reproducibility, re-useability, and applicability in clinical decision making. Here, the model construction pipeline and the SPARCED model contribute to this need by being built upon structured and annotated input files, by using open-source packages, and by being available publicly on GitHub.

One key advantage of the SPARCED model format its compatibility with RBM. The reactions and species created by RBM software can easily be incorporated (manually or programmatically) into the SPARCED model input files. In addition to the capabilities of rule-based modeling, the SPARCED models enable single rate parameter changes and inclusion/exclusion of individual rate laws. Then, the SPARCED-nf pipeline can be used to study large-scale variant analysis or to do parameter scanning. Combining this idea to test consistency across multiple datasets, users can search for best-fit models or pinpoint discrepant datasets given the model topology (28).

Another advantage of the SPARCED model is its ability to integrate multiple omics datasets into a large-scale mechanistic model, creating a “personalized” model variant reflective of another cellular or patient context (26,100). Users can incorporate mRNA, copy number variation (CNV), and even proteomics data from established databases like CCLE (101), TCGA (102–104), HPA (105–107), and Cellosaurus (108) into the input files programmatically (Fig. 3) and test changing the initial conditions of the model using the same network structure (Fig. 4). For instance, the SPARCED-I model can be trained on a dataset (RNAseq and RPPA) from LINCS Consortium (synapse.org/#!Synapse:syn12524705) to study the downstream signaling differences (i.e. AKT and MAPK cascades) of EGF, HGF, and IFNG stimulated MCF10A cells.

The SPARCED model encodes intrinsic stochasticity of total protein levels and mRNA numbers in its hybrid simulation mode, making it unique (together with the Bouhaddou2018 model) to offer stochastic as well as deterministic simulation settings. This single-cell capability allows one to capture some important aspects of cell line and tumor heterogeneity compared to an average cell condition (the way many mechanistic models are built). Users can leverage this feature to simulate virtual populations and study a cell population response to drug treatment, which is often a single-cell readout as are most cellular phenotypes. However, such simulation settings require larger computational resources and thus model compatibility for high performance computing environments. The SPARCED model is built to be compatible with cloud computing, where it can be used to simulate thousands of single cells with single job execution (see Methods).

There are, however, still some challenges to be addressed. One such task is to explore simulations of *spatially aware* single cells. Currently, the SPARCED model captures intrinsic heterogeneity of cells (by having stochastic gene switching and mRNA birth/death events) but these cells cannot “talk” to each other. In the future, by having scenarios where spatial orientation of cells are recorded and the secreted or stimulated molecules are shared between them, we can better capture tissue microenvironment. Related to this first task, the second challenge is to create and simulate scenarios with multiple cell types (i.e. models trained on data from different subtypes

of cells) or defining events to capture differentiation of cells. One big challenge is to be able to obtain single cell RNAseq and/or proteomic data, and to train SPARCED-like models using such data. Then, combining all together: spatially aware, single-cell level, large-scale mechanistic models trained on patient data, we can generate ever-better in-silico drug screening for personalized therapies. With our pipeline here, we took an important step towards this goal.

Another challenge to achieve using large-scale models is to get a whole-cell level mechanistic model for mammalian cells. With our approach, the SPARCED model can be enlarged using other small-scale models for pathways and mechanisms not currently included in the model. By utilizing the unit testing approach, one can then verify the model performance and get larger, more comprehensive models. We have made it to the point where the community now can contribute and create a complementary code (or Jupyter notebook) for model context-change and parameter tuning based on new experimental conditions.

Our introduced method of large-scale mechanistic model construction, and the SPARCED model as a basis, will enable researchers to more easily create and manipulate new model versions, test different mechanisms of action to interpret experimental observations, and change the model's cellular context. The models created by our pipeline can incorporate multiple (omics) datasets, providing non-"black-box" data integration and modeling. These SPARCED models additionally provide single-cell level simulations, compatibility with cloud computing, and human-interpretable & annotated model files in SBML format. The SPARCED model now can be re-used as one of the largest mammalian-cell mechanistic model in the literature and serves a primer role in creation of context-specific, hypotheses testing, and expandable models. In conclusion, the SPARCED model format contributes towards important foundations of reusable big models, paving the way towards personalized mechanistic models for data integration.

ACKNOWLEDGMENTS

The authors acknowledge funding from the National Institutes of Health Grants R01GM104184 and U54HG008098-LINCS Center (MRB), U54CA209988 and U54HG008100-LINCS Center (LMH), the National Science Foundation Grant CC*-1659300 (FAF), and portions of this work were performed under the auspices of the U.S. Department of Energy by Lawrence Livermore National Laboratory under Contract DE-AC52-07NA27344. LLNL-JOUR-###### (RCB). CE was an NIH-LINCS Postdoctoral Fellow.

REFERENCES

1. Wilkinson MD, Dumontier M, Aalbersberg IjJ, Appleton G, Axton M, Baak A, et al. The FAIR Guiding Principles for scientific data management and stewardship. Sci Data. 2016 Dec;3(1):160018.

2. Ma'ayan A, Rouillard AD, Clark NR, Wang Z, Duan Q, Kou Y. Lean Big Data integration in systems biology and systems pharmacology. Trends Pharmacol Sci. 2014 Sep;35(9):450–60.

3. Gomez-Cabrero D, Abugessaisa I, Maier D, Teschendorff A, Merkenschlager M, Gisel A, et al. Data integration in the era of omics: current and future challenges. BMC Syst Biol. 2014;8(Suppl 2):I1.

4. Stites EC, Aziz M, Creamer MS, Von Hoff DD, Posner RG, Hlavacek WS. Use of Mechanistic Models to Integrate and Analyze Multiple Proteomic Datasets. Biophys J. 2015 Apr;108(7):1819–29.

5. Mirza B, Wang W, Wang J, Choi H, Chung NC, Ping P. Machine Learning and Integrative Analysis of Biomedical Big Data. Genes. 2019 Jan 28;10(2):87.

6. Huang S, Chaudhary K, Garmire LX. More Is Better: Recent Progress in Multi-Omics Data Integration Methods. Front Genet. 2017 Jun 16;8:84.

7. Zeng ISL, Lumley T. Review of Statistical Learning Methods in Integrated Omics Studies (An Integrated Information Science). Bioinforma Biol Insights. 2018 Jan;12:117793221875929.

8. Jensen KJ, Janes KA. Modeling the latent dimensions of multivariate signaling datasets. Phys Biol. 2012 Aug 1;9(4):045004.

9. Adam G, Rampášek L, Safikhani Z, Smirnov P, Haibe-Kains B, Goldenberg A. Machine learning approaches to drug response prediction: challenges and recent progress. Npj Precis Oncol. 2020 Dec;4(1):19.

10. Ianevski A, Giri AK, Gautam P, Kononov A, Potdar S, Saarela J, et al. Prediction of drug combination effects with a minimal set of experiments. Nat Mach Intell. 2019 Dec;1(12):568–77.

11. Liu H, Zhang W, Nie L, Ding X, Luo J, Zou L. Predicting effective drug combinations using gradient tree boosting based on features extracted from drug-protein heterogeneous network. BMC Bioinformatics. 2019 Dec;20(1):645.

12. Wong D, Yip S. Machine learning classifies cancer. Nature. 2018 Mar;555(7697):446–7.

13. Ehteshami Bejnordi B, Veta M, Johannes van Diest P, van Ginneken B, Karssemeijer N, Litjens G, et al. Diagnostic Assessment of Deep Learning Algorithms for Detection of Lymph Node Metastases in Women With Breast Cancer. JAMA. 2017 Dec 12;318(22):2199.

14. Kleppe A, Albregtsen F, Vlatkovic L, Pradhan M, Nielsen B, Hveem TS, et al. Chromatin organisation and cancer prognosis: a pan-cancer study. Lancet Oncol. 2018 Mar;19(3):356–69.

15. Esteva A, Kuprel B, Novoa RA, Ko J, Swetter SM, Blau HM, et al. Dermatologist-level classification of skin cancer with deep neural networks. Nature. 2017 Feb 2;542(7639):115–8.

16. Yu MK, Ma J, Fisher J, Kreisberg JF, Raphael BJ, Ideker T. Visible Machine Learning for Biomedicine. Cell. 2018 Jun;173(7):1562–5.

17. Baker RE, Peña J-M, Jayamohan J, Jérusalem A. Mechanistic models versus machine learning, a fight worth fighting for the biological community? Biol Lett. 2018 May;14(5):20170660.

18. Najafabadi MM, Villanustre F, Khoshgoftaar TM, Seliya N, Wald R, Muharemagic E. Deep learning applications and challenges in big data analytics. J Big Data. 2015 Dec;2(1):1.

19. Wang F, Casalino LP, Khullar D. Deep Learning in Medicine—Promise, Progress, and Challenges. JAMA Intern Med. 2019 Mar 1;179(3):293.

20. Yang JH, Wright SN, Hamblin M, McCloskey D, Alcantar MA, Schrübbers L, et al. A White-Box Machine Learning Approach for Revealing Antibiotic Mechanisms of Action. Cell. 2019 May;177(6):1649-1661.e9.

21. Kholodenko BN, Hancock JF, Kolch W. Signalling ballet in space and time. Nat Rev Mol Cell Biol. 2010;11:414–426.

22. Carrera J, Covert MW. Why Build Whole-Cell Models? Trends Cell Biol. 2015 Dec;25(12):719–22.

23. Karr JR, Sanghvi JC, Macklin DN, Gutschow MV, Jacobs JM, Bolival Jr. B, et al. A whole-cell computational model predicts phenotype from genotype. Cell. 2012;150:389–401.

24. Carrera J, Elena SF, Jaramillo A. Computational design of genomic transcriptional networks with adaptation to varying environments. Proc Natl Acad Sci. 2012 Sep 18;109(38):15277–82.

25. Münzner U, Klipp E, Krantz M. A comprehensive, mechanistically detailed, and executable model of the cell division cycle in Saccharomyces cerevisiae. Nat Commun. 2019 Dec;10(1):1308.

26. Saez-Rodriguez J, Blüthgen N. Personalized signaling models for personalized treatments. Mol Syst Biol [Internet]. 2020 Jan [cited 2020 Jul 27];16(1). Available from: https://onlinelibrary.wiley.com/doi/abs/10.15252/msb.20199042

27. Halasz M, Kholodenko BN, Kolch W, Santra T. Integrating network reconstruction with mechanistic modeling to predict cancer therapies. Sci Signal. 2016;9(455):ra114.

28. Macklin DN, Ahn-Horst TA, Choi H, Ruggero NA, Carrera J, Mason JC, et al. Simultaneous cross-evaluation of heterogeneous E. coli datasets via mechanistic simulation. Science. 2020 24;369(6502).

29. Santos SDM, Verveer PJ, Bastiaens PIH. Growth factor-induced MAPK network topology shapes Erk response determining PC-12 cell fate. Nat Cell Biol. 2007 Mar;9(3):324–30.

30. Kholodenko BN, Demin OV, Moehren G, Hoek JB. Quantification of short term signaling by the epidermal growth factor receptor. J Biol Chem. 1999 Oct 15;274(42):30169–81.

31. Tyson JJ. Modeling the cell division cycle: cdc2 and cyclin interactions. Proc Natl Acad Sci. 1991 Aug 15;88(16):7328–32.

32. Nyman E, Fagerholm S, Jullesson D, Stralfors P, Cedersund G. Mechanistic explanations for counter-intuitive phosphorylation dynamics of the insulin receptor and insulin receptor substrate-1 in response to insulin in murine adipocytes. Febs J. 2012;279:987–999.

33. Schmierer B, Tournier AL, Bates PA, Hill CS. Mathematical modeling identifies Smad nucleocytoplasmic shuttling as a dynamic signal-interpreting system. Proc Natl Acad Sci. 2008 May 6;105(18):6608–13.

34. Vilar JMG, Guet CC, Leibler S. Modeling network dynamics. J Cell Biol. 2003 May 12;161(3):471–6.

35. Kofahl B, Klipp E. Modelling the dynamics of the yeast pheromone pathway. Yeast. 2004 Jul 30;21(10):831–50.

36. Tyson JJ, Chen K, Novak B. Network dynamics and cell physiology. Nat Rev Mol Cell Biol. 2001 Dec;2(12):908–16.

37. Puszyński K, Hat B, Lipniacki T. Oscillations and bistability in the stochastic model of p53 regulation. J Theor Biol. 2008 Sep;254(2):452–65.

38. Sedaghat AR, Sherman A, Quon MJ. A mathematical model of metabolic insulin signaling pathways. Am J Physiol Endocrinol Metab. 2002;283:E1084–101.

39. Carrera J, Estrela R, Luo J, Rai N, Tsoukalas A, Tagkopoulos I. An integrative, multi-scale, genome-wide model reveals the phenotypic landscape of *E scherichia coli* . Mol Syst Biol. 2014 Jul;10(7):735.

40. Bouhaddou M, Barrette AM, Stern AD, Koch RJ, DiStefano MS, Riesel EA, et al. A mechanistic pan-cancer pathway model informed by multi-omics data interprets stochastic cell fate responses to drugs and mitogens. PLoS Comput Biol [Internet]. 2018;14(3). Available from: http://journals.plos.org/ploscompbiol/article/file?id=10.1371/journal.pcbi.1005985&type=printable

41. Fröhlich F, Kessler T, Weindl D, Shadrin A, Schmiester L, Hache H, et al. Efficient Parameter Estimation Enables the Prediction of Drug Response Using a Mechanistic Pan-Cancer Pathway Model. Cell Syst. 2018 Dec;7(6):567-579.e6.

42. Dalle Pezze P, Sonntag AG, Thien A, Prentzell MT, Godel M, Fischer S, et al. A Dynamic Network Model of mTOR Signaling Reveals TSC-Independent mTORC2 Regulation. Sci Signal. 2012 Mar 27;5(217):ra25–ra25.

43. Capuani F, Conte A, Argenzio E, Marchetti L, Priami C, Polo S, et al. Quantitative analysis reveals how EGFR activation and downregulation are coupled in normal but not in cancer cells. Nat Commun. 2015 Nov;6(1):7999.

44. Orth JD, Thiele I, Palsson BØ. What is flux balance analysis? Nat Biotechnol. 2010 Mar;28(3):245–8.

45. Lee JM. Flux balance analysis in the era of metabolomics. Brief Bioinform. 2006 Mar 7;7(2):140–50.

46. Sherman MS, Cohen BA. A Computational Framework for Analyzing Stochasticity in Gene Expression. Morozov AV, editor. PLoS Comput Biol. 2014 May 8;10(5):e1003596.

47. Raj A, Peskin CS, Tranchina D, Vargas DY, Tyagi S. Stochastic mRNA Synthesis in Mammalian Cells. Schibler U, editor. PLoS Biol. 2006 Sep 12;4(10):e309.

48. Raj A, van Oudenaarden A. Nature, Nurture, or Chance: Stochastic Gene Expression and Its Consequences. Cell. 2008 Oct;135(2):216–26.

49. Faeder JR, Blinov ML, Goldstein B, Hlavacek WS. Rule-based modeling of biochemical networks. Complexity. 2005 Mar;10(4):22–41.

50. Harris LA, Hogg JS, Tapia JJ, Sekar JA, Gupta S, Korsunsky I, et al. BioNetGen 2.2: advances in rule-based modeling. Bioinformatics. 2016;32:3366–3368.

51. Xu W, Smith AM, Faeder JR, Marai GE. RuleBender: a visual interface for rule-based modeling. Bioinformatics. 2011;27:1721–1722.

52. Boutillier P, Maasha M, Li X, Medina-Abarca HF, Krivine J, Feret J, et al. The Kappa platform for rule-based modeling. Bioinformatics. 2018 Jul 1;34(13):i583–92.

53. Lopez CF, Muhlich JL, Bachman JA, Sorger PK. Programming biological models in Python using PySB. Mol Syst Biol. 2013;9.

54. Sneddon MW, Faeder JR, Emonet T. Efficient modeling, simulation and coarse-graining of biological complexity with NFsim. Nat Methods. 2011 Feb;8(2):177–83.

55. Hogg JS, Harris LA, Stover LJ, Nair NS, Faeder JR. Exact hybrid particle/population simulation of rule-based models of biochemical systems. PLoS Comput Biol. 2014 Apr;10(4):e1003544.

56. Goldberg AP, Szigeti B, Chew YH, Sekar JA, Roth YD, Karr JR. Emerging whole-cell modeling principles and methods. Curr Opin Biotechnol. 2017;51:97–102.

57. Porubsky VL, Goldberg AP, Rampadarath AK, Nickerson DP, Karr JR, Sauro HM. Best Practices for Making Reproducible Biochemical Models. Cell Syst. 2020 Aug;11(2):109–20.

58. Azeloglu EU, Iyengar R. Good practices for building dynamical models in systems biology. Sci Signal. 2015;8.

59. Hucka M, Finney A, Sauro HM, Bolouri H, Doyle JC, Kitano H, et al. The systems biology markup language (SBML): a medium for representation and exchange of biochemical network models. Bioinformatics. 2003 Mar 1;19(4):524–31.

60. Keating SM, Waltemath D, König M, Zhang F, Dräger A, Chaouiya C, et al. SBML Level 3: an extensible format for the exchange and reuse of biological models. Mol Syst Biol [Internet]. 2020 Aug [cited 2020 Oct 7];16(8). Available from: https://onlinelibrary.wiley.com/doi/abs/10.15252/msb.20199110

61. Hoops S, Sahle S, Gauges R, Lee C, Pahle J, Simus N, et al. COPASI--a COmplex PAthway SImulator. Bioinformatics. 2006 Dec 15;22(24):3067–74.

62. Loew LM, Schaff JC. The Virtual Cell: a software environment for computational cell biology. Trends Biotechnol. 2001 Oct;19(10):401–6.

63. Smith LP, Bergmann FT, Chandran D, Sauro HM. Antimony: a modular model definition language. Bioinformatics. 2009 Sep 15;25(18):2452–4.

64. Rensin DK. Kubernetes-scheduling the future at cloud scale. 2015;

65. Thurgood B, Lennon RG. Cloud Computing With Kubernetes Cluster Elastic Scaling. In: Proceedings of the 3rd International Conference on Future Networks and Distributed Systems - ICFNDS '19 [Internet]. Paris, France: ACM Press; 2019 [cited 2020 Sep 22]. p. 1–7. Available from: http://dl.acm.org/citation.cfm?doid=3341325.3341995

66. Smarr L, Crittenden C, DeFanti T, Graham J, Mishin D, Moore R, et al. The Pacific Research Platform: Making High-Speed Networking a Reality for the Scientist. In: Proceedings of the Practice and Experience on Advanced Research Computing [Internet]. Pittsburgh PA USA: ACM; 2018 [cited 2020 Sep 22]. p. 1–8. Available from: https://dl.acm.org/doi/10.1145/3219104.3219108

67. Fröhlich F, Theis FJ, Rädler JO, Hasenauer J. Parameter estimation for dynamical systems with discrete events and logical operations. Bioinformatics. 2016 Dec 31;btw764.

68. Kluyver T, Ragan-Kelley B, Pérez F, Granger B, Bussonnier M, Frederic J, et al. Jupyter Notebooks – a publishing format for reproducible computational workflows. In: Loizides F, Schmidt B, editors. Positioning and Power in Academic Publishing: Players, Agents and Agendas. IOS Press; 2016. p. 87–90.

69. Fröhlich F, Kaltenbacher B, Theis FJ, Hasenauer J. Scalable Parameter Estimation for Genome-Scale Biochemical Reaction Networks. Stelling J, editor. PLOS Comput Biol. 2017 Jan 23;13(1):e1005331.

70. Bouhaddou M, Birtwistle MR. Dimerization-based control of cooperativity. Mol BioSyst. 2014;10(7):1824–32.

71. Birtwistle MR, Hatakeyama M, Yumoto N, Ogunnaike BA, Hoek JB, Kholodenko BN. Ligand-dependent responses of the ErbB signaling network: experimental and modeling analyses. Mol Syst Biol. 2007 Jan;3(1):144.

72. Albeck JG, Burke JM, Spencer SL, Lauffenburger DA, Sorger PK. Modeling a Snap-Action, Variable-Delay Switch Controlling Extrinsic Cell Death. Levchenko A, editor. PLoS Biol. 2008 Dec 2;6(12):e299.

73. Nakakuki T, Birtwistle MR, Saeki Y, Yumoto N, Ide K, Nagashima T, et al. Ligand-Specific c-Fos Expression Emerges from the Spatiotemporal Control of ErbB Network Dynamics. Cell. 2010 May;141(5):884–96.

74. von Kriegsheim A, Baiocchi D, Birtwistle M, Sumpton D, Bienvenut W, Morrice N, et al. Cell fate decisions are specified by the dynamic ERK interactome. Nat Cell Biol. 2009 Dec;11(12):1458–64.

75. Gerard C, Goldbeter A. Temporal self-organization of the cyclin/Cdk network driving the mammalian cell cycle. Proc Natl Acad Sci. 2009 Dec 22;106(51):21643–8.

76. Batchelor E, Loewer A, Mock C, Lahav G. Stimulus-dependent dynamics of p53 in single cells. Mol Syst Biol. 2011 Jan;7(1):488.

77. Hindmarsh AC, Brown PN, Grant KE, Lee SL, Serban R, Shumaker DE, et al. SUNDIALS: Suite of nonlinear and differential/algebraic equation solvers. ACM Trans Math Softw TOMS. 2005 Sep;31(3):363–96.

78. Yates AD, Achuthan P, Akanni W, Allen J, Allen J, Alvarez-Jarreta J, et al. Ensembl 2020. Nucleic Acids Res. 2019 Nov 6;gkz966.

79. Braschi B, Denny P, Gray K, Jones T, Seal R, Tweedie S, et al. Genenames.org: the HGNC and VGNC resources in 2019. Nucleic Acids Res. 2019 Jan 8;47(D1):D786–92.

80. Weindl D, Fröhlich F, Stapor P, Schälte Y, AMICI-Developer, LeonardSchmiester, et al. ICB-DCM/AMICI: AMICI v0.11.2 [Internet]. Zenodo; 2020 [cited 2020 Jul 27]. Available from: https://zenodo.org/record/3949231

81. Yamada S, Shiono S, Joo A, Yoshimura A. Control mechanism of JAK/STAT signal transduction pathway. FEBS Lett. 2003 Jan 16;534(1–3):190–6.

82. Sullivan DM, Latham MD, Ross WE. Proliferation-dependent topoisomerase II content as a determinant of antineoplastic drug action in human, mouse, and Chinese hamster ovary cells. Cancer Res. 1987 Aug 1;47(15):3973–9.

83. Torgerson TR, Colosia AD, Donahue JP, Lin YZ, Hawiger J. Regulation of NF-kappa B, AP-1, NFAT, and STAT1 nuclear import in T lymphocytes by noninvasive delivery of peptide carrying the nuclear localization sequence of NF-kappa B p50. J Immunol Baltim Md 1950. 1998 Dec 1;161(11):6084–92.

84. Tsai C-C, Kai J-I, Huang W-C, Wang C-Y, Wang Y, Chen C-L, et al. Glycogen Synthase Kinase-3β Facilitates IFN-γ-Induced STAT1 Activation by Regulating Src Homology-2 Domain-Containing Phosphatase 2. J Immunol. 2009 Jul 15;183(2):856–64.

85. Angel P, Hattori K, Smeal T, Karin M. The jun proto-oncogene is positively autoregulated by its product, Jun/AP-1. Cell. 1988 Dec 2;55(5):875–85.

86. Meissl K, Macho-Maschler S, Müller M, Strobl B. The good and the bad faces of STAT1 in solid tumours. Cytokine. 2017 Jan;89:12–20.

87. Schroder K, Hertzog PJ, Ravasi T, Hume DA. Interferon-γ: an overview of signals, mechanisms and functions. J Leukoc Biol. 2004 Feb;75(2):163–89.

88. Parker BS, Rautela J, Hertzog PJ. Antitumour actions of interferons: implications for cancer therapy. Nat Rev Cancer. 2016 Mar;16(3):131–44.

89. Townsend PA, Scarabelli TM, Davidson SM, Knight RA, Latchman DS, Stephanou A. STAT-1 Interacts with p53 to Enhance DNA Damage-induced Apoptosis. J Biol Chem. 2004 Feb 13;279(7):5811–20.

90. Koromilas AE, Sexl V. The tumor suppressor function of STAT1 in breast cancer. JAK-STAT. 2013 Apr;2(2):e23353.

91. Seif F, Khoshmirsafa M, Aazami H, Mohsenzadegan M, Sedighi G, Bahar M. The role of JAK-STAT signaling pathway and its regulators in the fate of T helper cells. Cell Commun Signal. 2017 Dec;15(1):23.

92. Hilton DJ. Negative regulators of cytokine signal transduction. Cell Mol Life Sci CMLS. 1999 Oct 2;55(12):1568–77.

93. Pawson T, Gish GD, Nash P. SH2 domains, interaction modules and cellular wiring. Trends Cell Biol. 2001 Dec 1;11(12):504–11.

94. Huang H, Li L, Wu C, Schibli D, Colwill K, Ma S, et al. Defining the Specificity Space of the Human Src Homology 2 Domain. Mol Cell Proteomics. 2008 Apr;7(4):768–84.

95. Böhmer F-D, Friedrich K. Protein tyrosine phosphatases as wardens of STAT signaling. JAK-STAT. 2014 Jan 21;3(1):e28087.

96. Tseng P-C, Huang W-C, Chen C-L, Sheu B-S, Shan Y-S, Tsai C-C, et al. Regulation of SHP2 by PTEN/AKT/GSK-3β signaling facilitates IFN-γ resistance in hyperproliferating gastric cancer. Immunobiology. 2012 Sep;217(9):926–34.

97. Wang S, Wang N, Yu B, Cao M, Wang Y, Guo Y, et al. Circulating IGF-1 promotes prostate adenocarcinoma via FOXO3A/BIM signaling in a double-transgenic mouse model. Oncogene. 2019 Sep;38(36):6338–53.

98. Weeks KL, Bernardo BC, Ooi JYY, Patterson NL, McMullen JR. The IGF1-PI3K-Akt Signaling Pathway in Mediating Exercise-Induced Cardiac Hypertrophy and Protection. In: Xiao J, editor. Exercise for Cardiovascular Disease Prevention and Treatment: From Molecular to Clinical, Part 2 [Internet]. Singapore: Springer Singapore; 2017. p. 187–210. Available from: https://doi.org/10.1007/978-981-10-4304-8_12

99. Melnik BC, John SM, Schmitz G. Over-stimulation of insulin/IGF-1 signaling by Western diet may promote diseases of civilization: lessons learnt from Laron syndrome. Nutr Metab. 2011 Jun 24;8(1):41.

100. Barrette AM, Bouhaddou M, Birtwistle MR. Integrating Transcriptomic Data with Mechanistic Systems Pharmacology Models for Virtual Drug Combination Trials. ACS Chem Neurosci. 2018 Jan 17;9(1):118–29.

101. Barretina J, Caponigro G, Stransky N, Venkatesan K, Margolin AA, Kim S, et al. The Cancer Cell Line Encyclopedia enables predictive modelling of anticancer drug sensitivity. Nature. 2012 Mar;483(7391):603–7.

102. Cancer Genome Atlas Research N. Comprehensive genomic characterization defines human glioblastoma genes and core pathways. Nature. 2008;455:1061–1068.

103. Cancer Genome Atlas Research N, Weinstein JN, Collisson EA, Mills GB, Shaw KR, Ozenberger BA, et al. The Cancer Genome Atlas Pan-Cancer analysis project. Nat Genet. 2013;45:1113–1120.

104. Hutter C, Zenklusen JC. The Cancer Genome Atlas: Creating Lasting Value beyond Its Data. Cell. 2018 Apr;173(2):283–5.

105. Uhlen M, Fagerberg L, Hallstrom BM, Lindskog C, Oksvold P, Mardinoglu A, et al. Tissue-based map of the human proteome. Science. 2015 Jan 23;347(6220):1260419–1260419.

106. Thul PJ, Åkesson L, Wiking M, Mahdessian D, Geladaki A, Ait Blal H, et al. A subcellular map of the human proteome. Science. 2017 May 26;356(6340):eaal3321.

107. Uhlen M, Zhang C, Lee S, Sjöstedt E, Fagerberg L, Bidkhori G, et al. A pathology atlas of the human cancer transcriptome. Science. 2017 Aug 18;357(6352):eaan2507.

108. Bairoch A. The Cellosaurus, a Cell-Line Knowledge Resource. J Biomol Tech JBT. 2018 Jul;29(2):25–38.

Figure/Table Legends

Figure 1. SPARCED is a structured, human interpretable, and easy to modify big mechanistic model. (A) The schematic of the underlying model for SPARCED. Image adapted from (40). (B) The pan-cancer mechanistic model Bouhaddou2018 is re-written in open-source and structured file format. The steps of model construction include input file creation and conversion into an SBML file. The annotated SBML model file and stochastic module are simulated together at single-cell level locally or by using cloud-computing. The benefits of the new SPARCED model include easy alteration and expansion capabilities through text file editing, human-readable annotated input files, and use of Jupyter-notebooks for model creation and simulation. The modeling pipeline introduced here are inline with good practices of re-usable big mechanistic models (57). (C) The Bouhaddou2018 model file types are simplified and converted into open-source platforms.

Table 1. List of SPARCED model unit testing and comparisons to Bouhaddou2018 model. The SPARCED model passed each test depicted below and recapitulated experimental and simulation observations reported by the Bouhaddou2018 model.

Figure 2. SPARCED model recapitulates experimental observations and deterministic/hybrid (deterministic + stochastic) simulation results of the Bouhaddou2018 model. (A) Summary of comparisons of SPARCED model deterministic simulations to Bouhaddou2018 model simulations. The area under the curve (AUC) values of each simulation (see Fig. S12) are calculated and plotted for the two model results. (B) Simulation results from Bouhaddou2018 model and SPARCED-nf model (lines) run on Kubernetes cluster workflow are the same as SPARCED model (circle) results. Comparisons of selected panels from (A) are shown only. (C) Experimental and stochastic simulation results from Bouhaddou 2018 model are reproduced by SPARCED model simulations. Each dot is a different condition, explained in Figure S131A. Error bars show experimental or simulation standard error of the mean. Simulations are of at least 100 cells, and three independent experimental observations where applicable. (D) Stochastic simulation of 100 cells recapture protein level trajectories (active p53, Cyclin A, and cPARP) from older model qualitatively. Panels with blue background are SPARCED simulations and white background panels are from Bouhaddou2018 model. 100 stochastic cells are stimulated with EGF+Insulin for 72 hours before Etoposide treatment for another 72 hours. Etoposide is stimulated also with EGF+Insulin. Results for Etoposide treatment without prior growth factor stimulations are shown in Figure S13B. (E) Quantification of results in (D) shows that SPARCED model simulations coincide with earlier observations in percentage of death

induced by etoposide treatment. See Figure S13C for the effect of no growth factor stimulation before Etoposide treatment. Bars represent mean ± s.e.m.

Figure 3. **SPARCED model alteration guidelines.** (A) Steps of model expansion and context change procedures are listed. Refer to Table 2 for more details. Steps can be skipped if no changes are necessary. (B) The list of parameters and species values modified for SPARCED model context change from MCF10A cells to U87 cells. (C) SPARCED_U87 model simulations reproduce previous observations, where U87 cells show increased response and sensitivity to AKT inhibition. MEKi: MEK inhibitor, AKTi: AKT inhibitor. Bars represent mean ± s.e.m. of 100 single cell simulations for each condition.

Table 2. SPARCED model alteration steps.

Figure 4. SPARCED model is enlarged to include interferon-gamma (IFNG) signaling pathway. (A) Experiments showed that IFNG treatment decreases cell proliferation induced by EGF alone. Fraction of EdU positive cells at 48 hours after EGF alone or EGF+IFNG treatment are calculated. Bars represent mean ± s.e.m of three independent biological replicates. (B) Yamada2003 model schematic of IFNG pathway added into SPARCED model. (C) Overview of the added IFNG-IFNGR pathway in relation to the Bouhaddou2018 model pathways. The “mech1 and mech2” links are candidate mechanisms tested in the next section. (D) Simulations of the Yamada2003 model, SPARCED-I model, and SPARCED-I model with MCF10A context show qualitative and quantitative agreements. The Yamada2003 model results (blue diamonds) are obtained by running the model file in COPASI (XXX). (E) 100 stochastic cell simulations (area plots) and the deterministic (dashed-black lines) simulation of 10 nM IFNG stimulation are shown. Colored dark lines represent median cell trajectories, dark and light-colored regions represent 70th and 95th quantiles, respectively. The right-most plot shows mRNA count of SOCS1 in each cell, colored differently.

Figure 5. Study of SPARCED-I model enabled us to propose how IFNG treatment decreases cell proliferation induced by EGF. (A) Experimental setup and simulation workflow for SPARCED-I model variant analysis. See Methods. (B) Candidate mechanism schematic 1: activated STAT1 induces p21 transcription. (C) Candidate mechanism schematic 2: SOCS1 sequesters activated ligand-receptor complexes. (D) Simulation of 100 stochastic cells for SPARCED-I-mech1 and (E) SPARCED-I-mech2 models showed that SOCS1 sequestration of activated receptor complexes can better explain the IFNG effect on cell proliferation inhibition, compared to experiments shown in Fig. 4A. The bar plots show the total number Cyclin A peaks

calculated at specified time points for the starting 100 cells. (F) Normalized p21 levels do not show a significant change when IFNG is included in addition to the EGF. (G) Normalized ppAKT levels show a significant decrease after IFNG treatment, when EGF+IFNG Mechanism 2 simulations are compared to EGF alone case. RPPA data are shown in black error lines, from three independent replicates. Colored dark lines represent median cell trajectories from simulations, dark and light-colored regions represent 70th and 95th quantiles, respectively. * indicates p-value < 0.05, *** indicates p-value < 0.001. (F-G) Data from synapse.org/#!Synapse:syn12526172.

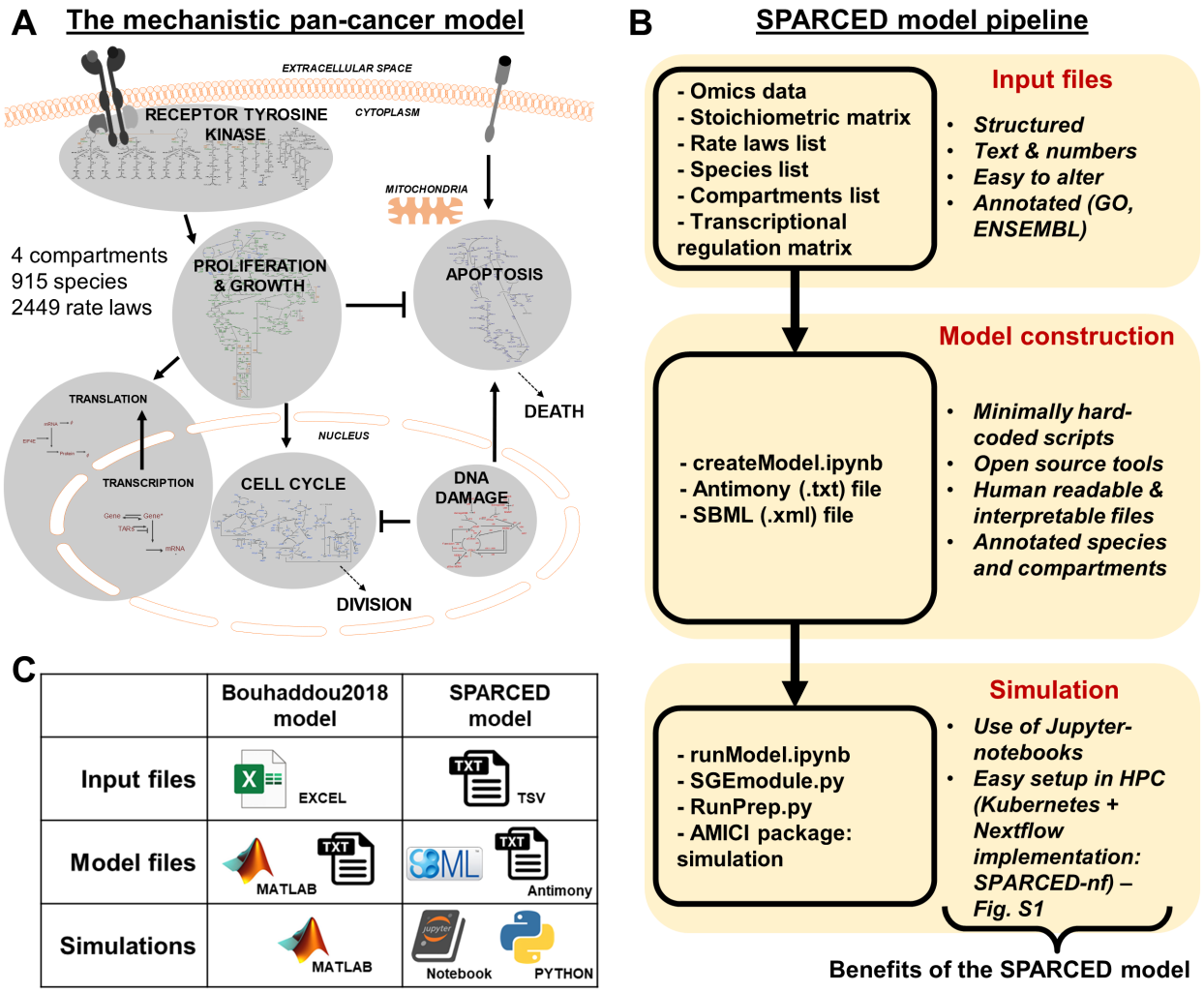
A
The mechanistic pan-cancer model
EXTRACELLULAR SPACE
RECEPTOR TYROSINE KINASE
CYTOPLASM
MITOCHONDRIA
4 compartments
915 species
2449 rate laws
PROLIFERATION & GROWTH
APOPTOSIS
TRANSLATION
DEATH
NUCLEUS
TRANSCRIPTION
CELL CYCLE
DNA DAMAGE
DIVISION
B
SPARCED model pipeline
- Omics data
- Stoichiometric matrix
- Rate laws list
- Species list
- Compartments list
- Transcriptional regulation matrix
Input files
Structured
Text & numbers
Easy to alter
Annotated (GO, ENSEMBL)
Model construction
- createModel.ipynb
- Antimony (.txt) file
- SBML (.xml) file
Minimally hard-coded scripts
Open source tools
Human readable & interpretable files
Annotated species and compartments
Simulation
- runModel.ipynb
- SGEmodule.py
- RunPrep.py
- AMICI package: simulation
Use of Jupyter-notebooks
Easy setup in HPC (Kubernetes + Nextflow implementation: SPARCED-nf) – Fig. S1
Benefits of the SPARCED model
C
Bouhaddou2018 model
SPARCED model
Input files
EXCEL
TSV
Model files
MATLAB
Antimony
Simulations
MATLAB
Notebook
PYTHON

Descriptions of unit tests	Simulation type	Figure #	Original paper Figure #
Functional test to ensure the deterministic module is updated every 30 seconds with mRNA numbers generated by the stochastic module.	Stochastic	Fig. S2	2B
Simulated ligand-receptor cooperativity coefficients for the receptor tyrosine kinases match experimental observations (negative cooperativity: EGF, FGF, IGF, INS; no cooperativity: HGF, NRG1, and positive cooperativity: PDGF).	Deterministic	Fig. S3A	3A + S3A
Activated EGF receptors internalize and peak ~30 minutes after ligand treatment.	Deterministic	Fig. S3B	S3B
EGF and insulin stimulation activates both ERK and AKT pathways. Dual stimulation with the two ligands induces prolonged AKT activation.	Deterministic	Figs. S4-5	3B,C,D + S3C
Double and/or single stranded DNA damage activates p53 and DNA damage repair mechanisms represses its response.	Deterministic	Fig. S6A	3E
Increasing DNA damage amount in single cells leads to higher number of activated p53 peaks.	Stochastic	Fig. S6B-C	3F + S3E
Increasing simulated TRAIL dose decreases the time it takes to die for an average cell.	Deterministic	Fig. S7A-B	3G
The fraction of surviving cells decreases as stimulated TRAIL dose increases.	Stochastic	Fig. S7C	3H
Increasing ERK and AKT activity levels prolongs TRAIL induced time to death, whereas increasing PUMA and NOXA expression levels decreases the time it takes for cells to die.	Deterministic	Fig. S7D	3I
Increasing Cyclin D mRNA levels induces proper cyclin-CDK complex progression and oscillations for cell cycle entry and progression.	Deterministic	Fig. S8A	3J
Etoposide treatment induces cell cycle arrest and cell death. Cycling cells (with prior growth factor stimulation) show increased percentage of death to etoposide treatment, compared to non-cycling cells.	Stochastic	**Fig. 2D-E**	4A,B,C
Inhibition of AKT and ERK pathways together synergistically increase cell death, in EGF and insulin stimulated cells.	Stochastic	Fig. S9	5A
ERK and AKT inhibition induced cell death mechanisms are predominantly BIM dependent, not BAD dependent.	Stochastic	Fig. S10A	5C
EGF and insulin cooperatively induce cell cycle entry, with insulin inducing very little cell cycle entry alone.	Stochastic	Fig. S10B	6B
Activation of both ERK and AKT pathways are required for robust cell cycle entry. Time averaged ppERK and ppAKT levels correlate with Cyclin D levels.	Deterministic	Fig. S11	6E
The number of ribosomes within the cell doubles within 24 hours.	Deterministic	Fig. S8B	S2D

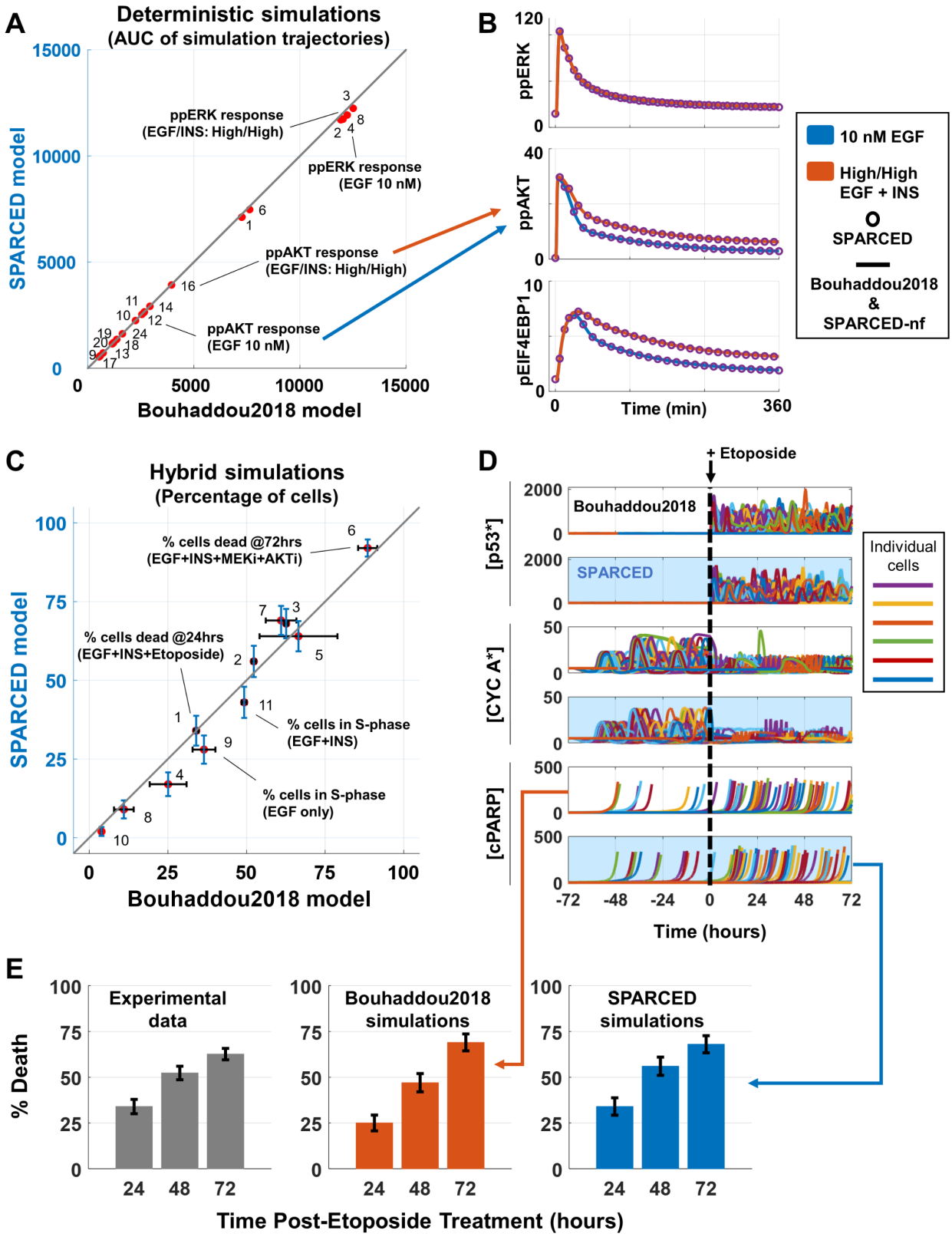
A
Deterministic simulations
(AUC of simulation trajectories)
SPARCED model
Bouhaddou2018 model
ppERK response
(EGF/INS: High/High)
ppERK response
(EGF 10 nM)
ppAKT response
(EGF/INS: High/High)
ppAKT response
(EGF 10 nM)
B
ppERK
ppAKT
pEIF4EBP1
Time (min)
10 nM EGF
High/High
EGF + INS
SPARCED
Bouhaddou2018
&
SPARCED-nf
C
Hybrid simulations
(Percentage of cells)
SPARCED model
Bouhaddou2018 model
% cells dead @72hrs
(EGF+INS+MEKi+AKTi)
% cells dead @24hrs
(EGF+INS+Etoposide)
% cells in S-phase
(EGF+INS)
% cells in S-phase
(EGF only)
D
+ Etoposide
Bouhaddou2018
SPARCED
[p53*]
[CYC A*]
[cPARP]
Individual
cells
Time (hours)
E
% Death
Experimental
data
Bouhaddou2018
simulations
SPARCED
simulations
Time Post-Etoposide Treatment (hours)

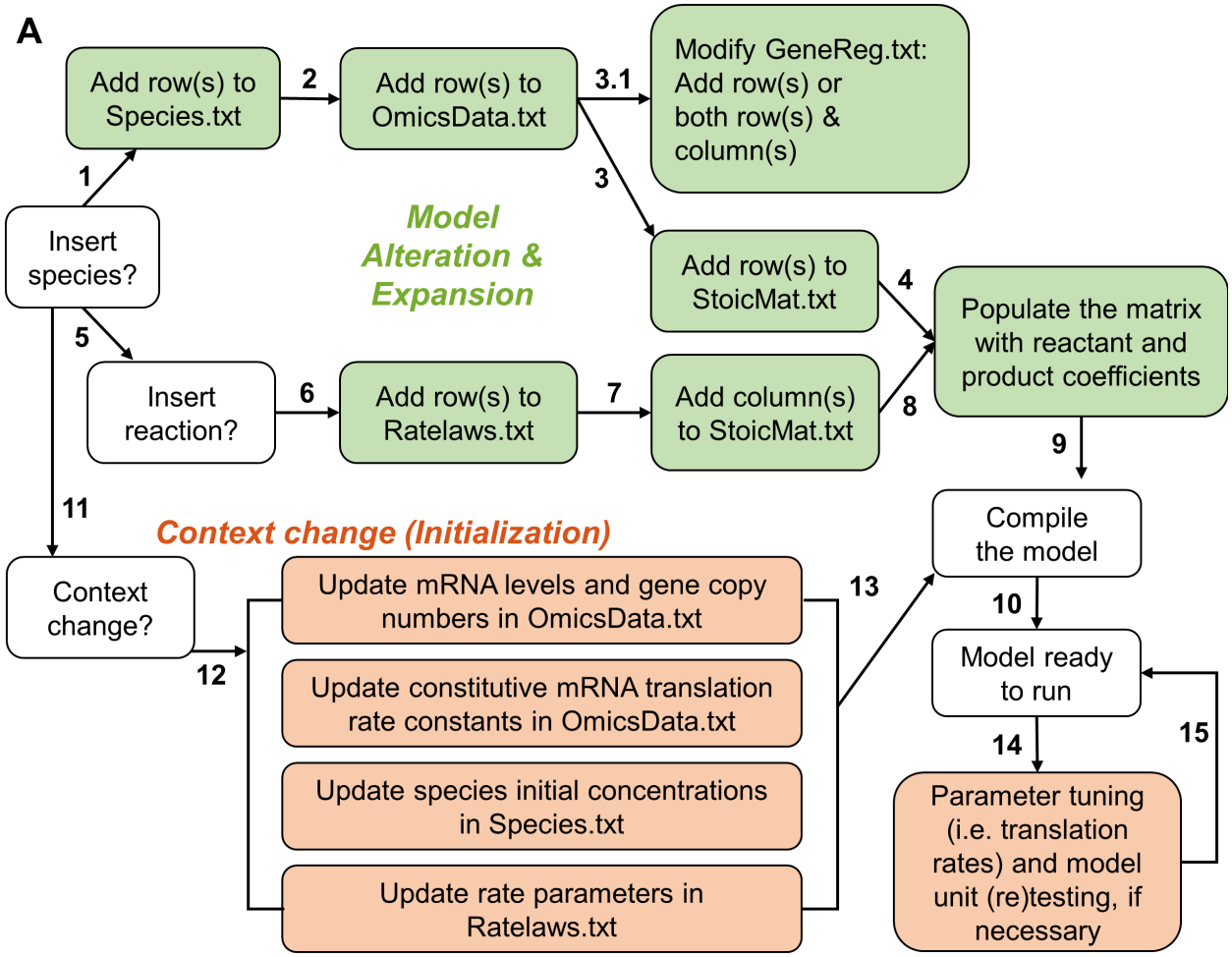

B

Parameter category changed	Number of parameters changed (out of 3275 possible)	Input file
mRNA counts	141	OmicsData.txt
Gene copy numbers	141	OmicsData.txt
Constitutive mRNA translation rates	141	OmicsData.txt
Induced mRNA translation rates (from Bouhaddou2018)	141	Ratelaws.txt
Degradation rate constants (from Bouhaddou2018)	46	Ratelaws.txt
Species initial concentrations (from Bouhaddou2018)	914 (out of 914)	Species.txt

C

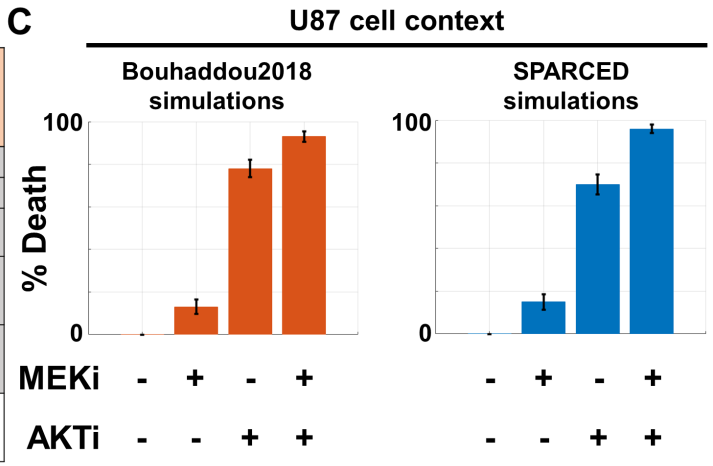

SPARCED model expansion protocol		SPARCED model context change protocol	
1	Decide if you need to add a new species, and a row to Species.txt for each new one.	**11**	If no changes in model topology are required, and a model context change (i.e. cell type) is desired, no new rows and columns are added.
2	Define if the new species has a new gene and add a row to OmicsData.txt file. If the new species is a product of existing gene, no alteration in OmicsData.txt required.	**12a**	Update the OmicsData.txt file with new data of mRNA levels and gene copy numbers.
3	Add each new species as a new row to StoicMat.txt file.	**12b**	Update the OmicsData.txt file with constitutive mRNA translation rate constants.
3.1	If the new species has a new gene, define if it has a transcriptional activator and/or repressor. If No, add only row(s) in GeneReg.txt, with all zeros as the column values. If Yes, add row(s) to define the new gene(s) and column(s) to define the effector species. Define the transcriptional regulation parameters by entering non-zero values in the new row(s)/column(s).	**12c**	Update species initial concentrations in Species.txt file. The concentrations here are steady-state values (e.g. *Initialized* values from Bouhaddou2018 model, determined by training the model using cell line specific omics data).
4	Set the new species' stoichiometric coefficient for each reaction in StoicMat.txt file.	**12d**	Update rate-law parameter values in Ratelaws.txt. This step could include a small number of manual alterations, like turning-off a reaction.
5	Decide if you need to add a new reaction to the model (if not, skip to 9).	**13**	Compile the new model, using WriteModel.ipynb Jupyter-notebook.
6	Add a new row for each new reaction to the Ratelaws.txt and set the corresponding rate parameters.	**10**	Run the new model.
7	Add a new column for each new reaction to the StoicMat.txt.	**14**	Employ parameter tuning (i.e. translation and degradation rates), using the model created with new initial conditions and simulations. Model unit (re)testing is recommended.
8	Define the reactants & products of each new reaction and set their stoichiometric coefficients StoicMat.txt file.	**15**	Run the new model.
9	Compile the new model topology, using WriteModel.ipynb Jupyter-notebook.		
10	Run the new model.		

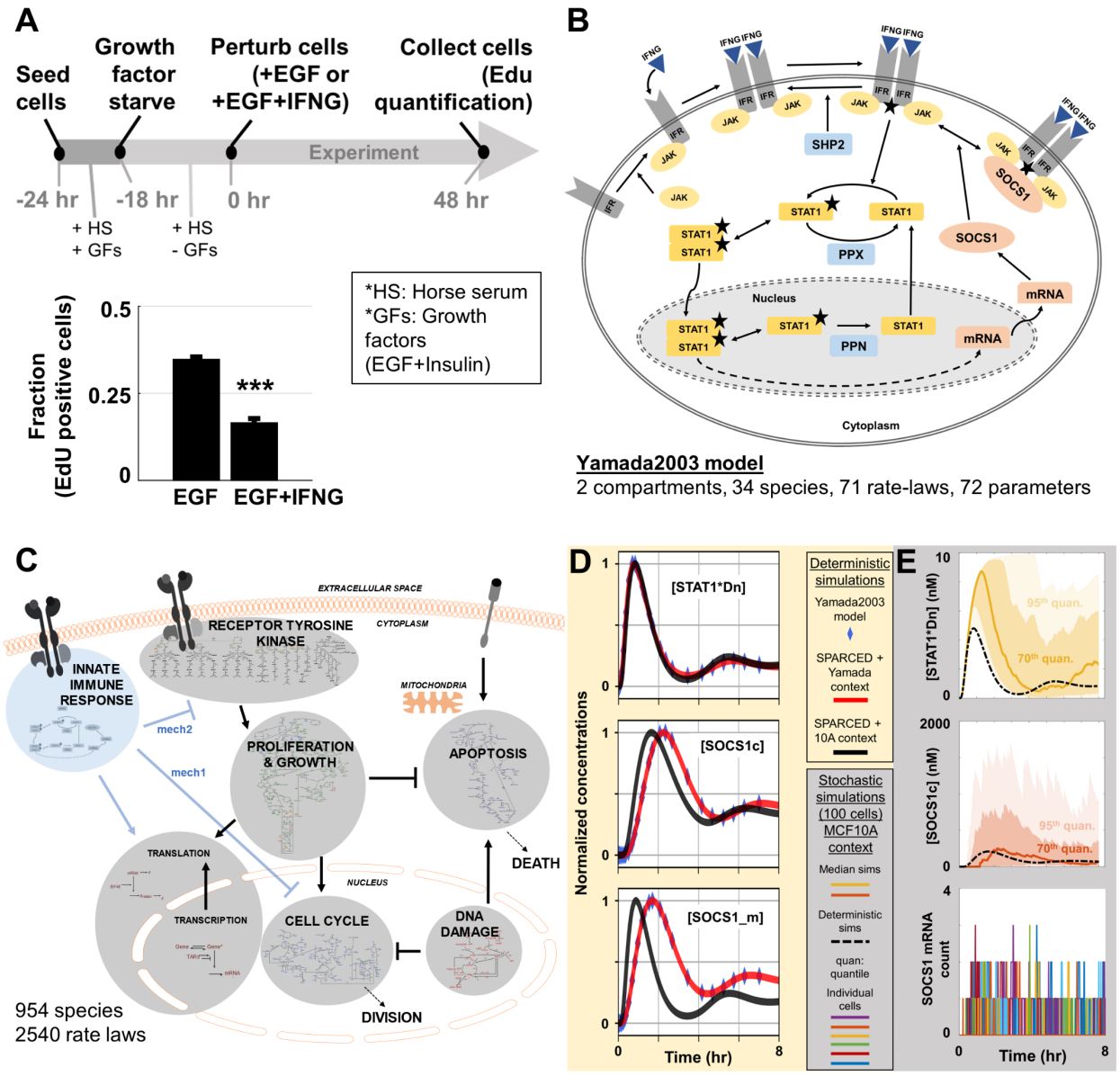
A
Seed cells
Growth factor starve
Perturb cells (+EGF or +EGF+IFNG)
Collect cells (Edu quantification)
Experiment
-24 hr
-18 hr
0 hr
48 hr
+ HS
+ GFs
+ HS
- GFs
Fraction (EdU positive cells)
0.5
0.25
0
***
EGF
EGF+IFNG
*HS: Horse serum
*GFs: Growth factors (EGF+Insulin)
B
IFNG
IFR
JAK
SHP2
STAT1
PPX
SOCS1
mRNA
Nucleus
PPN
Cytoplasm
Yamada2003 model
2 compartments, 34 species, 71 rate-laws, 72 parameters
C
EXTRACELLULAR SPACE
CYTOPLASM
RECEPTOR TYROSINE KINASE
INNATE IMMUNE RESPONSE
MITOCHONDRIA
mech2
mech1
PROLIFERATION & GROWTH
APOPTOSIS
DEATH
TRANSLATION
TRANSCRIPTION
NUCLEUS
CELL CYCLE
DNA DAMAGE
DIVISION
954 species
2540 rate laws
D
[STAT1*Dn]
[SOCS1c]
[SOCS1_m]
Normalized concentrations
Time (hr)
Deterministic simulations
Yamada2003 model
SPARCED + Yamada context
SPARCED + 10A context
Stochastic simulations (100 cells) MCF10A context
Median sims
Deterministic sims
quan: quantile
Individual cells
E
[STAT1*Dn] (nM)
95th quan.
70th quan.
[SOCS1c] (nM)
SOCS1 mRNA count
Time (hr)

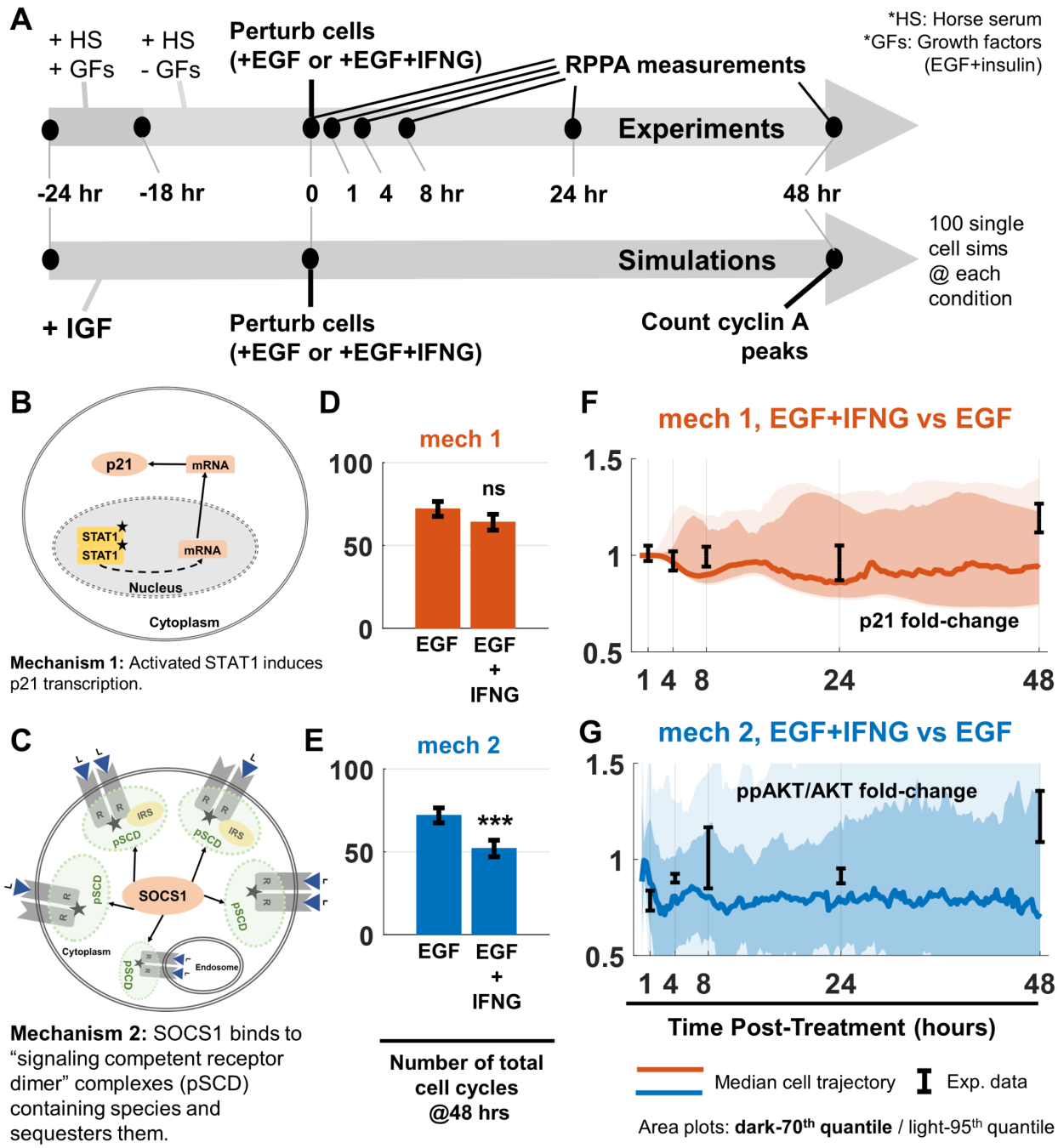
A
+ HS
+ GFs
+ HS
- GFs
Perturb cells
(+EGF or +EGF+IFNG)
RPPA measurements
*HS: Horse serum
*GFs: Growth factors
(EGF+insulin)
Experiments
-24 hr
-18 hr
0
1
4
8 hr
24 hr
48 hr
100 single
cell sims
@ each
condition
Simulations
+ IGF
Perturb cells
(+EGF or +EGF+IFNG)
Count cyclin A
peaks
B
p21
mRNA
STAT1
STAT1
mRNA
Nucleus
Cytoplasm
Mechanism 1: Activated STAT1 induces p21 transcription.
D
mech 1
100
50
0
ns
EGF
EGF + IFNG
F
mech 1, EGF+IFNG vs EGF
1.5
1
0.5
p21 fold-change
1 4 8
24
48
C
SOCS1
IRS
pSCD
Cytoplasm
Endosome
Mechanism 2: SOCS1 binds to "signaling competent receptor dimer" complexes (pSCD) containing species and sequesters them.
E
mech 2
100
50
0
***
EGF
EGF + IFNG
Number of total cell cycles @48 hrs
G
mech 2, EGF+IFNG vs EGF
1.5
1
0.5
ppAKT/AKT fold-change
1 4 8
24
48
Time Post-Treatment (hours)
Median cell trajectory
Exp. data
Area plots: dark-70th quantile / light-95th quantile